Article

Gut microbiota modulates weight gain in mice after discontinued smoke exposure

https://doi.org/10.1038/s41586-021-04194-8

Received: 25 August 2020

Accepted: 28 October 2021

Published online: 08 December 2021

Check for updates

Leviel Fluhr[1,8], Uria Mor[1,8], Aleksandra A. Kolodziejczyk[1], Mally Dori-Bachash[1], Avner Leshem[1,2], Shlomik Itav[1], Yotam Cohen[1], Jotham Suez[1], Niv Zmora[1,3,4], Claudia Moresi[1], Shahar Molina[1], Niv Ayalon[1], Rafael Valdés-Mas[1], Shanni Hornstein[1], Hodaya Karbi[1], Denise Kviatcovsky[1], Adi Livne[1], Aurelie Bukimer[1], Shimrit Eliyahu-Miller[1], Alona Metz[1], Alexander Brandis[5], Tevie Mehlman[5], Yael Kuperman[6], Michael Tsoory[6], Noa Stettner[6], Alon Harmelin[6], Hagit Shapiro[1,9]✉ & Eran Elinav[1,7,9]✉

Cigarette smoking constitutes a leading global cause of morbidity and preventable death[1], and most active smokers report a desire or recent attempt to quit[2]. Smoking-cessation-induced weight gain (SCWG; 4.5 kg reported to be gained on average per 6–12 months, >10 kg year^{-1} in 13% of those who stopped smoking[3]) constitutes a major obstacle to smoking abstinence[4], even under stable[5,6] or restricted[7] caloric intake. Here we use a mouse model to demonstrate that smoking and cessation induce a dysbiotic state that is driven by an intestinal influx of cigarette-smoke-related metabolites. Microbiome depletion induced by treatment with antibiotics prevents SCWG. Conversely, fecal microbiome transplantation from mice previously exposed to cigarette smoke into germ-free mice naive to smoke exposure induces excessive weight gain across diets and mouse strains. Metabolically, microbiome-induced SCWG involves a concerted host and microbiome shunting of dietary choline to dimethylglycine driving increased gut energy harvest, coupled with the depletion of a cross-regulated weight-lowering metabolite, *N*-acetylglycine, and possibly by the effects of other differentially abundant cigarette-smoke-related metabolites. Dimethylglycine and *N*-acetylglycine may also modulate weight and associated adipose-tissue immunity under non-smoking conditions. Preliminary observations in a small cross-sectional human cohort support these findings, which calls for larger human trials to establish the relevance of this mechanism in active smokers. Collectively, we uncover a microbiome-dependent orchestration of SCWG that may be exploitable to improve smoking-cessation success and to correct metabolic perturbations even in non-smoking settings.

Smoking[8–10] and smoking cessation[5,8] might be associated with gut microbiome alterations, but no studies have causally linked these dysbiotic changes to SCWG. To explore this possibility, we utilized a mouse model whereby mice fed a high-fat diet (HFD) or a normal chow diet (NC) were placed in a smoking chamber to expose them to cigarette smoke (Methods). Exact statistical values, including *P* values and linear mixed model (LMM) parameters (Methods) are provided in Supplementary Table 1. Data are provided as the percent weight change, which reflects the rate of weight gain relative to the baseline weight of each mouse. Absolute weights and individual experimental repeats are also depicted in Supplementary Information 1 and 2, respectively. Using this smoke exposure model, the plasma nicotine level of HFD-fed mice exposed to smoke was 5.51 ± 1.32 ng ml^{-1} (mean ± s.e.m.), which is comparable to levels reported in human active smokers[11,12]. Acute exposure to cigarette smoke induced a significant reduction in weight that was associated with other metabolic features (Extended Data Fig. 1). By contrast, mice no longer exposed to smoke had SCWG that was comparable to weight levels of mice not exposed to smoke. These results are similar to those described in human SCWG settings[13,14] (Extended Data Fig. 1b; LMM $P = 5.96 \times 10^{-13}$).

To determine whether the microbiome affects SCWG, 10-week-old C57BL/6 male mice fed a HFD were given a combination of four antibiotics accessible ad libitum through their drinking water (Methods, Fig. 1a). Both antibiotic-treated and non-treated mice exposed to smoke had lower weight gain compared with antibiotic-treated and non-treated mice not exposed to smoke (Fig. 1b, pooled results, four independent repeats). Notably, antibiotic-treated mice previously exposed to smoke had significantly lower SCWG and attenuated weight gain rate compared with non-antibiotic-treated mice previously exposed to smoke (Fig. 1b, c; LMM $P = 2.05 \times 10^{-9}$). This effect was persistent for 119 days

[1]Immunology Department, Weizmann Institute of Science, Rehovot, Israel. [2]Department of Surgery, Tel Aviv Sourasky Medical Center, Tel Aviv, Israel. [3]Research Center for Digestive Tract and Liver Diseases, Tel Aviv Sourasky Medical Center, Sackler Faculty of Medicine, Tel Aviv University, Tel Aviv, Israel. [4]Internal Medicine Department, Tel Aviv Sourasky Medical Center, Tel Aviv, Israel. [5]Department of Biological Services, Weizmann Institute of Science, Rehovot, Israel. [6]Department of Veterinary Resources, Weizmann Institute of Science, Rehovot, Israel. [7]Division of Cancer-Microbiome Research, DKFZ, Heidelberg, Germany. [8]These authors contributed equally: Leviel Fluhr, Uria Mor. [9]These authors jointly supervised this work: Hagit Shapiro, Eran Elinav. ✉e-mail: hagit.shapiro@weizmann.ac.il; eran.elinav@weizmann.ac.il

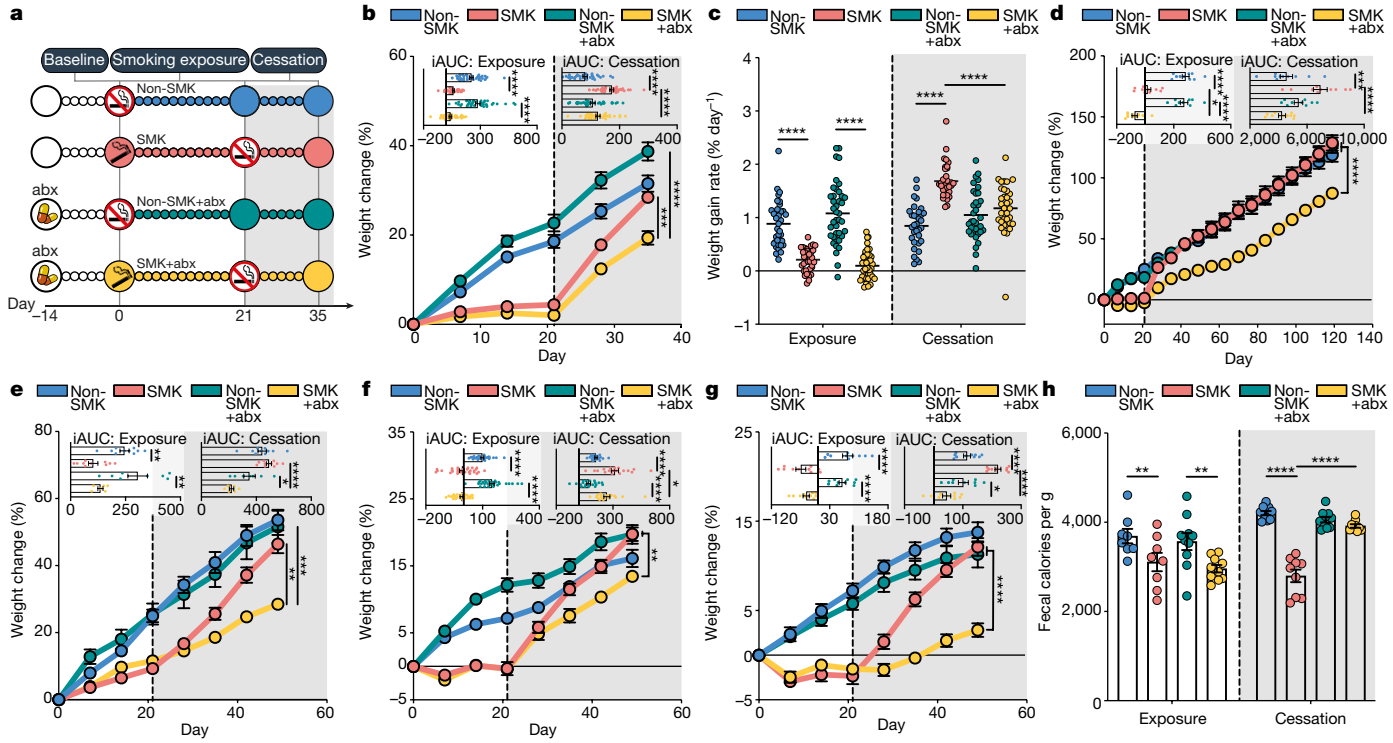

Fig. 1 | Microbiome depletion modulates SCWG. a, Experimental scheme. Mice were not exposed to cigarette smoke (non-SMK), exposed to smoke (SMK) and treated or not treated with antibiotics (abx) at the indicated time points. SMK groups were exposed to cigarette smoke for 3 weeks. **b**, Weight change in HFD-fed mice subjected to different treatments: non-SMK ($n = 37$), SMK ($n = 38$), non-SMK+abx ($n = 40$) and SMK+abx ($n = 39$). Results pooled from four independent repeats. For the last day, one-way analysis of variance (ANOVA) and Sidak correction was performed; inset shows incremental area under the curve (iAUC) weight change at smoke exposure (Exposure) or at cessation of smoke exposure (Cessation) sessions, one-way ANOVA and Sidak correction. This also applies to **d**–**g**. **c**, Weight gain rate, derivative calculated from exposure to smoke (Exposure) or cessation of smoke exposure (Cessation) time as Δweight change/Δdays. $n = 37$ (non-SMK), 38 (SMK), 40 (non-SMK+abx) or 39 (SMK+abx) mice; two-way analysis of variance (ANOVA) and Benjamini–Hochberg (BH) correction. Results pooled from four independent repeats. **d**, Long-term weight change in HFD-fed mice exposed to smoke and cessation over time. $n = 10$ (non-SMK, SMK and SMK+abx) or 9 (non-SMK+abx) mice. **e**, Weight change during smoke exposure and cessation in HFD-fed mice from a different vendor (The Jackson Laboratory). $n = 10$ (non-SMK and SMK), 8 (non-SMK+abx) or 6 (SMK+abx) mice. **f**, Weight change during smoke exposure and cessation in NC-fed mice. $n = 30$ mice per group, results pooled from 3 independent repeats. **g**, Weight change during smoke exposure and cessation in NC-fed mice exposed to low-nicotine cigarettes. $n = 10$ mice per group. **h**, Caloric content per g of stool in HFD-fed mice exposed to smoke and cessation. The following number of mice were used: non-SMK, smoke exposure $n = 8$, cessation $n = 10$; SMK, smoke exposure $n = 8$, cessation $n = 9$; non-SMK+abx, smoke exposure $n = 10$, cessation $n = 10$; SMK+abx, smoke exposure $n = 10$, cessation $n = 9$. Three-way ANOVA and BH correction. For all panels, grey backgrounds indicate the smoke-exposure cessation period, and all data are shown as the mean ± s.e.m. $^{*}P < 0.05$, $^{**}P < 0.01$, $^{***}P < 0.001$, $^{****}P < 0.0001$, exact P values presented in Supplementary Table 1.

of follow-up (Fig. 1d; LMM $P = 5.5 \times 10^{-19}$). Whole-body compositional analysis by nuclear magnetic resonance imaging supported these results (Extended Data Fig. 2a). Restricting the administration of antibiotics to the cessation period of smoke exposure did not alter SCWG (Extended Data Fig. 2b), which suggests that the antibiotic-induced effects observed during the period of acute smoke exposure are crucial for their ensuing impact on SCWG. HFD-fed wild-type mice obtained from a different vendor (The Jackson Laboratory, Methods, Fig. 1e; LMM $P = 8.21 \times 10^{-15}$) or mice fed with NC diet (Fig. 1f; LMM $P = 0.008124$, pooled results from 3 independent repeats) corroborated the effect of antibiotic-mediated abrogation of SCWG. NC- or HFD-fed mice exposed to smoke from low-nicotine cigarettes (Methods, Fig. 1g and Extended Data Fig. 2c, respectively) or HFD-fed mice exposed to smoke from high-nicotine cigarettes and 0.5 mg kg^{-1} day^{-1} varenicline (a competitive nicotinic receptor antagonist[15]; Extended Data Fig. 2d) generated a similar SCWG phenotype to that of mice exposed to smoke from high-nicotine cigarettes. The SCWG in these mice was abrogated by treatment with antibiotics (Fig. 1g; LMM $P = 1.74 \times 10^{-14}$).

Locomotion, total caloric intake and respiratory exchange ratio were comparable between antibiotic-treated and non-treated HFD-fed mice exposed or not exposed to smoke (Extended Data Fig. 3a–c). By contrast, energy expenditure (kcal h^{-1} kg^{-1}) was higher in mice during the cessation period of smoke exposure compared with control mice (not exposed to smoke) or antibiotic-treated mice that were no longer exposed to smoke (Extended Data Fig. 3d), despite their increased weight gain (Fig. 1b). Energy harvest, representing the level of energy extracted by the host from a given diet[16], was higher in HFD-fed mice exposed to smoke or previously exposed to smoke compared with control mice (as reflected by lower fecal residual calories). By contrast, treatment of mice previously exposed to smoke with antibiotics prevented this high energy harvest (Fig. 1h). A significant pair-wise correlation was noted between fecal caloric count to the rate of weight gain in mice previously exposed to smoke, but not in antibiotic-treated mice previously exposed to smoke (Extended Data Fig. 3e). This result suggests that enhanced energy harvest depends on the microbiome and is associated with SCWG. Collectively, these results imply that there is a microbiome-dependent, nicotine withdrawal-independent SCWG phenotype that is potentially driven by enhanced energy harvest from the host.

Smoking alters the gut microbiome

16S rDNA sequencing of fecal samples from HFD-fed mice exposed to cigarette smoke revealed that the mice had a dysbiotic configuration

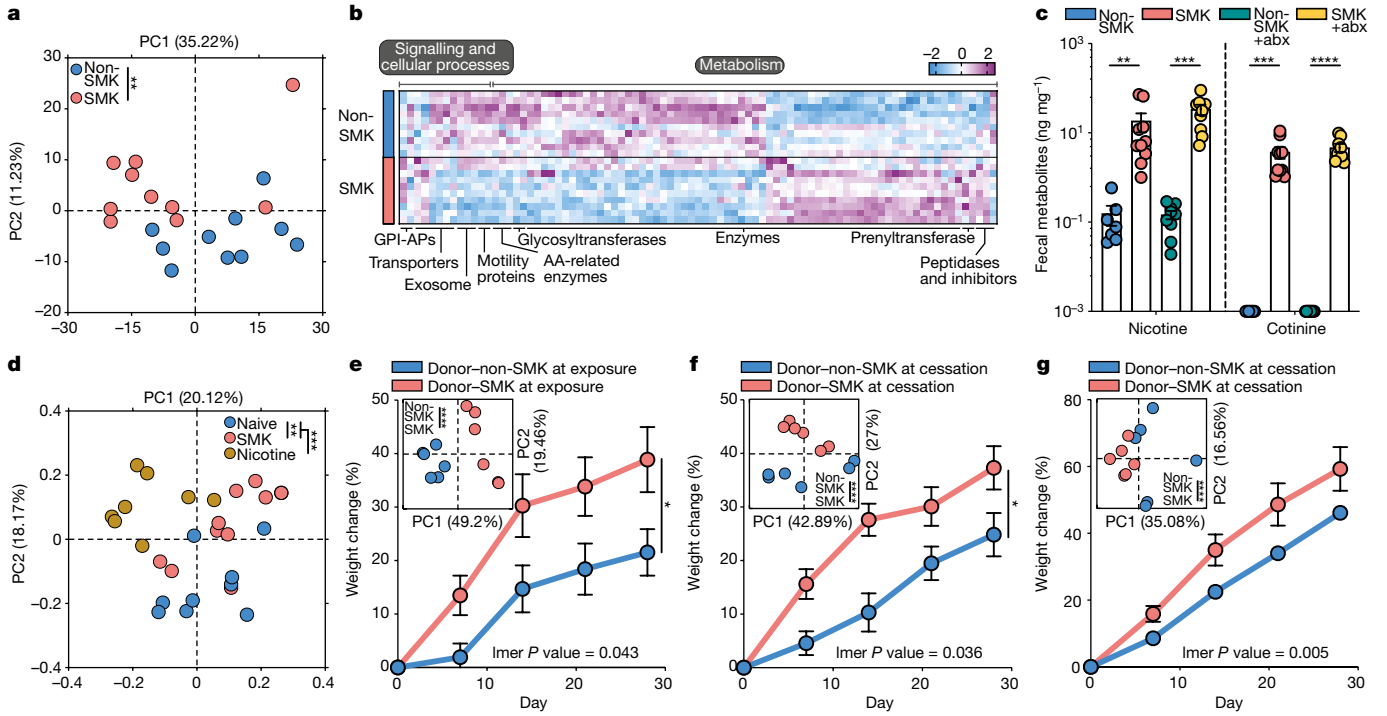

Fig. 2 | Cigarette-smoke-induced dysbiosis drives SCWG. a, Principal component analysis (PCA) of species-level relative abundance at day 21 (shotgun metagenomics). $n = 10$ HFD-fed mice per group; inset shows pairwise permutational analysis of variance (PERMANOVA). **b**, Heatmap of significantly different ($Q < 0.05$, DESeq2) metagenomic functional features (EC annotations) for HFD-fed mice exposed/not exposed to smoke at day 21. Features are grouped according to BRITE hierarchy ($n = 10$ mice per group). AA, amino acids; GPI-APs, glycosylphosphatidylinositol-anchored proteins. Coloured bar denotes z score. **c**, Fecal nicotine and cotinine levels during smoke exposure in HFD-fed mice. $n = 7$ (non-SMK), 10 (SMK) or 9 mice (non-SMK+abx and SMK+abx); Kruskal–Wallis and Dunn's test (mean ± s.e.m.). **d**, 16S rDNA principal coordinate analysis showing Bray–Curtis dissimilarity of mice exposed to smoke compared with nicotine-treated mice. All mice were fed with HFD, $n = 9$ (naive), 10 (SMK) or 8 nicotine-treated (intraperitoneal) mice. Inset shows pairwise PERMANOVA result. **e**–**g**, Weight change in HFD-fed GF recipients following FMT from HFD-fed mice after long exposure to smoke (**e**, day 18) or cessation (**f**, **g**, day 24). Non-SMK versus SMK unpaired two-sided t-test for day 28 (mean ± s.e.m.). Upper-left insets show PCA of species composition (sequenced $n = 6$ of each group in each experiment), PERMANOVA. P values of LMM using lmer test are presented in each panel. **e**, Recipients were SW mice, $n = 6$ per group (non-SMK and SMK). **f**, Recipients were SW mice, $n = 10$ (non-SMK) or 12 (SMK). **g**, Recipients were C57BL/6 mice, $n = 6$ (non-SMK) or 7 (SMK). $^*P < 0.05$, $^{**}P < 0.01$, $^{***}P < 0.001$, $^{****}P < 0.0001$, exact P values are presented in Supplementary Table 1.

within 3 weeks after acute smoke exposure (Extended Data Fig. 4a, b, Supplementary Table 2). Potential functional inference using phylogenetic investigation of communities by reconstruction of unobserved states (PICRUSt2)[17] revealed significant alterations in multiple genes between pre-smoke exposure and smoke exposure periods (pre-smoke exposure = 443, smoke exposure = 577, 26 shared; Supplementary Table 2), including the following 4 expanded Kyoto Encyclopedia of Genes and Genomes (KEGG) modules: cytochrome bc_1 complex respiratory unit (M00151); fatty acid biosynthesis, elongation (M00083); beta-oxidation-acyl, CoA synthesis (M00086); and betaine biosynthesis, choline to betaine (M00555) (Extended Data Fig. 4c). Shotgun metagenomic sequencing of fecal samples from HFD-fed mice exposed to smoke demonstrated that smoke exposure does not affect bacterial alpha diversity (Extended Data Fig. 4d). However, it does induce distinct compositional signatures (Fig. 2a) from a non-distinct baseline configuration (Extended Data Fig. 4e, Supplementary Table 3). These microbiome alterations did not fully revert to their pre-smoke exposure configurations 2 weeks following cessation of smoke exposure (Extended Data Fig. 4f, Supplementary Table 3). Of note, bacterial diversity was modified as a result of antibiotic treatment regardless of smoke exposure (Extended Data Fig. 4g). Dysbiosis during smoke exposure was characterized by distinct taxonomic (Extended Data Fig. 4h, Supplementary Table 3) and functional (Fig. 2b, Supplementary Table 3) metagenomic signatures, as determined by shotgun metagenomic sequencing.

To assess whether cigarette-smoke-related bioactive compounds are able to reach the intestines and affect the microbiome, we focused on nicotine as an exemplary metabolite that is systemically released during cigarette smoking while not being affected by microbiome presence (Extended Data Fig. 5a). Higher fecal (Fig. 2c) and plasma (Extended Data Fig. 5b) levels of nicotine and its main breakdown product cotinine were detected in both antibiotic-treated and non-treated HFD-fed mice exposed to smoke than in HFD-fed control (no smoke exposure) mice. Intraperitoneal nicotine supplementation (1.5 mg kg^{-1} day^{-1}; Extended Data Fig. 5c) twice a day for 3 weeks in HFD-fed mice induced a distinct dysbiotic state compared with both control mice and mice exposed to smoke (Fig. 2d, Extended Data Fig. 5d, Supplementary Table 2). However, weight reduction was only observed in mice that underwent acute exposure to smoke (Extended Data Fig. 5e). Oral nicotine administration (0.15 mg ml^{-1} in drinking water) for 3 weeks or continuous subcutaneous nicotine administration (1.5 mg kg^{-1} day^{-1} through osmotic pumps) for 4 weeks corroborated these findings (Extended Data Fig. 5f–j). Collectively, these results suggest that cigarette-smoke-related metabolites, such as nicotine, can modulate the gut microbiome under our tested conditions. Other nicotine doses and cigarette-smoke-released metabolites that may affect the microbiome merit future studies.

Causal microbiome involvement in SCWG

To investigate causative gut microbiome roles in SCWG, we performed fecal microbiome transplantation (FMT), in which fecal samples from mice exposed to smoke (Extended Data Fig. 6a) and mice previously exposed to smoke (Extended Data Fig. 6e) were transferred into different strains of germ-free (GF) mice naive to smoke exposure.

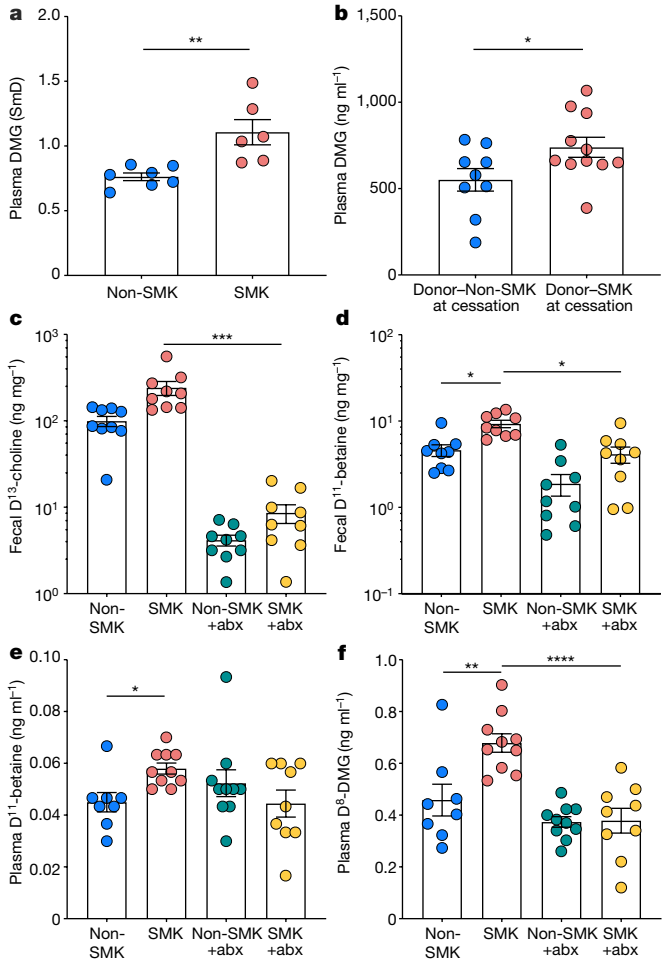

Fig. 3 | DMG dynamics during smoke exposure and cessation. a, Plasma DMG levels measured by untargeted mass spectrometry. Results are presented as a scaled imputed dataset (SmD). $n = 7$ (non-SMK) or 6 (SMK); HFD-fed mice. Two-sided unpaired *t*-test. **b**, Plasma DMG levels of GF HFD-fed mice receiving fecal transplant from HFD-fed mice at cessation, non-SMK ($n = 9$) or SMK ($n = 11$). Two-sided unpaired *t*-test. **c**–**f**, Targeted mass spectrometry analysis of HFD-fed mice gavaged with D^{13}-choline sulfate. Fecal and plasma samples were collected 4 h after administration and assessed for fecal D^{13}-choline (**c**) fecal D^{11}-betaine (**d**) plasma D^{11}-betaine (**e**) and plasma D^{8}-DMG (**f**). Fecal samples, $n = 9$ mice per group. Plasma samples, $n = 8$ (non-SMK), 10 (SMK and non-SMK+abx) or 9 mice (SMK+abx). Kruskal–Wallis and Dunn's test (**c**–**e**) and one-way ANOVA and Sidak (**f**). All data show the mean ± s.e.m. $^{*}P < 0.05$, $^{**}P < 0.01$, $^{***}P < 0.001$, $^{****}P < 0.0001$, exact *P* values are presented in Supplementary Table 1.

Microbiomes transferred from HFD-fed C57BL/6 mice exposed to cigarette smoke for 7 days into HFD-fed GF Swiss Webster (SW) mice or into HFD-fed GF C57BL/6 mice (neither exposed to smoke) induced dysbiosis in recipient mice that did not result in significant weight gain (Extended Data Fig. 6b, c, Supplementary Table 3). Microbiomes transferred from NC-fed C57BL/6 mice exposed to smoke for 7 days into NC-fed GF C57BL/6 mice not exposed to smoke produced similar results (Extended Data Fig. 6d, Supplementary Table 3). By contrast, microbiomes transferred from HFD-fed C57BL/6 mice exposed to smoke for 18 days into HFD-fed GF SW mice not exposed to smoke induced both compositional dysbiosis and excessive weight gain in recipient mice (Fig. 2e; $P = 0.0428$). Similar results were observed for microbiomes transferred from C57BL/6 mice during the cessation period of smoke exposure (day 24) into HFD-fed GF SW recipient mice not exposed to smoke (Fig. 2f; LMM P = 0.0356)), HFD-fed GF C57BL/6 recipients not exposed to smoke (Fig. 2g; LMM P = 0.00482) or NC-fed GF C57BL/6 recipients not exposed to smoke (Extended Data Fig. 6f). Taxonomic (Extended Data Fig. 6g) and functional (Extended Data Fig. 7a) analyses of recipient fecal samples demonstrated shared features of the altered microbiome (Supplementary Table 3).

Next, we pretreated HFD- or NC-fed donor mice with broad-spectrum antibiotics (Methods) during the entire smoke-exposure period and cessation of smoke-exposure period and then performed FMT into GF mice not exposed to smoke. These recipient mice had reduced weight gain compared with mice that received a smoking-cessation microbiome (Extended Data Fig. 7b, c). HFD-fed recipient GF mice colonized with microbiomes from mice that underwent a 7-day smoke exposure featured a comparable fecal caloric contents to that of recipients of microbiomes from control mice (not exposed to smoke, Extended Data Fig. 7d). By contrast, GF mouse recipients of microbiomes obtained at the smoking-cessation period had reduced fecal caloric content as compared to recipients of microbiomes from control mice (Extended Data Fig. 7e). This result suggests that there is increased energy harvest in recipients of microbiomes collected during smoking cessation, compared with recipients of microbiomes from control mice not exposed to smoke. Collectively, these data imply that the cigarette-smoke-induced dysbiotic microbiome gradually acquires a functional capacity to induce weight gain and enhance energy harvest, which becomes fully apparent during smoking cessation.

Microbiome-modulated metabolites in SCWG

We used untargeted mass spectrometry (Methods) to profile the plasma (Extended Data Fig. 8a) and fecal (Extended Data Fig. 8b) metabolites (Supplementary Table 4) in HFD-fed mice during acute smoke exposure (day 15 for plasma and day 21 for stool) and during cessation of smoke exposure (day 30 for plasma and day 35 for stool). A LMM (Extended Data Fig. 8c, Methods) analysis identified the following seven candidate metabolites that correlated with a microbiome-induced SCWG: *N*-formylanthranilic acid, trigonelline (*N*′-methylnicotinate), dimethylglycine (DMG), *N*-acetylglycine (aceturic acid (ACG)), hexadecadienoate (16:2n6), 1-palmitoyl-2-gamma-linolenoyl-GPC (16:0/18:3n6) and hexanoylglycine (Supplementary Table 5). DMG, a derivative of the amino acid glycine, can be synthesized from dietary choline sulfate by conversion into choline, betaine aldehyde, betaine and DMG through a series of enzymatic steps. These enzymes predominantly occur in the gut microbiome (choline sulfatase) and either the microbiome or the host (choline dehydrogenase, betaine-aldehyde dehydrogenase and betaine-homocysteine *S*-methyltransferase (BHMT)[18]). We used PICRUSt2[17] to infer functional abundance in the microbiome, and the results showed that the choline sulfate-betaine biosynthetic pathway (M00555; Extended Data Fig. 4c) and its key enzyme choline-*O*-sulfatase (Extended Data Fig. 8d) are upregulated during acute smoke exposure. Moreover, untargeted metabolomics showed a modest increase in fecal choline (Extended Data Fig. 8e) and a significant increase in betaine (Extended Data Fig. 8f) in HFD-fed mice exposed to smoke compared with HFD-fed mice not exposed to smoke. Expression of BHMT, which mediates the conversion of betaine to DMG, was undetected in stool, but was significantly increased in livers of mice exposed to smoke compared with those from mice not exposed to smoke (Extended Data Fig. 8g). This result suggests that increased cigarette-smoke-induced betaine-to-DMG conversion driving high systemic DMG levels (Fig. 3a) may be contributed by the host. Targeted mass spectrometry demonstrated that plasma DMG levels in HFD-fed mice exposed to smoke were reduced after antibiotic treatment (Extended Data Fig. 8h). Moreover, higher plasma DMG levels were observed in HFD-fed GF mice that received FMT from donors that underwent cessation of smoke exposure compared with FMT recipients from control mice not exposed to smoke (Fig. 3b). Together, these results further corroborate the role of the microbiome in this cigarette-smoke-modulated biosynthetic pathway. To validate these findings, HFD-fed mice exposed to smoke for 21 days were orally gavaged with tagged-choline sulfate (D^{13}-choline sulfate, Methods),

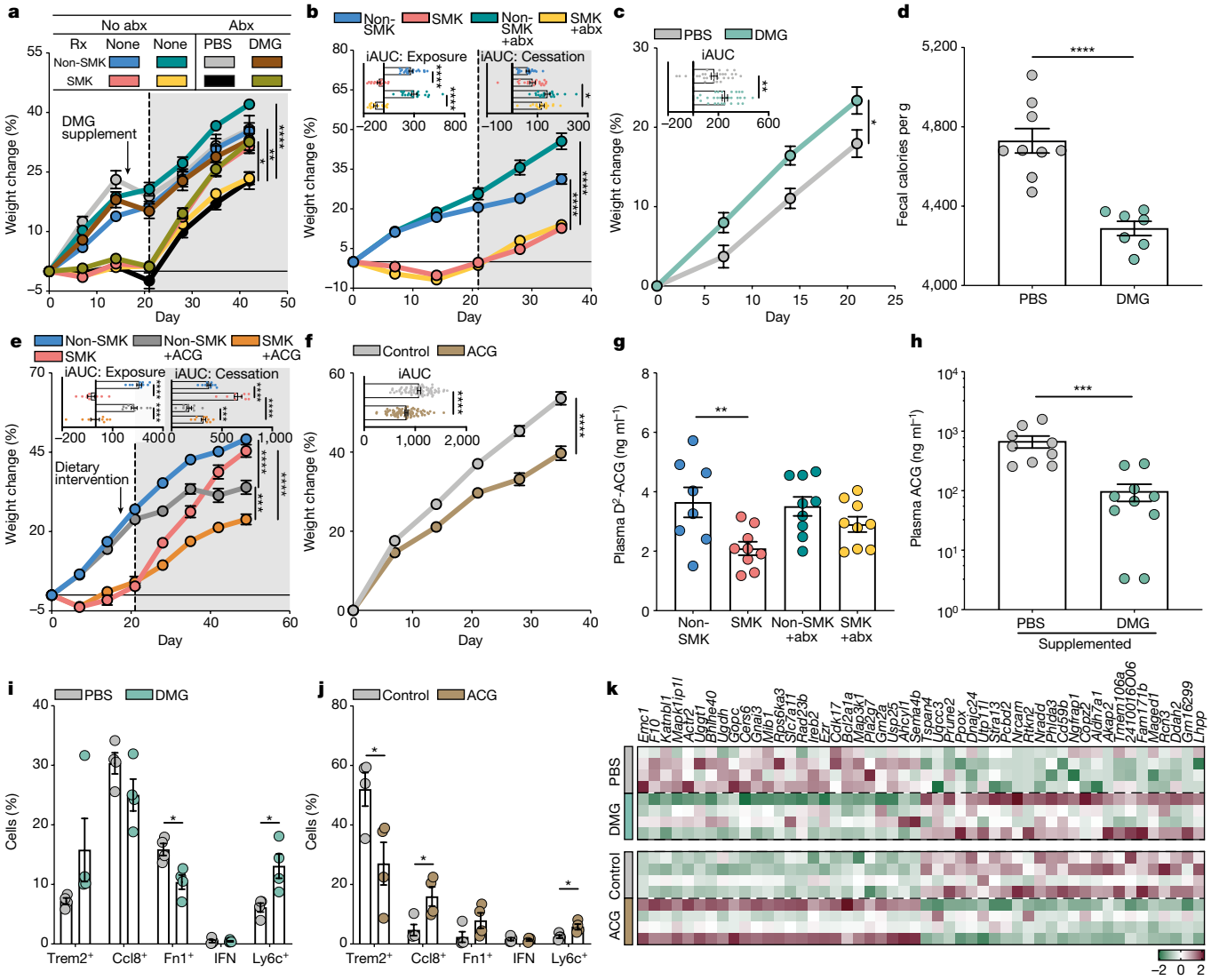

Fig. 4 | Cigarette-smoke-related metabolites affect SCWG. a, SCWG of HFD-fed mice supplemented with DMG. $n = 10$ per group except non-SMK+abx ($n = 9$); day 42: one-way ANOVA and Sidak. Rx, treatment. **b**, Weight change during smoke exposure and cessation in mice fed a choline-deficient diet. $n = 20$ (non-SMK, SMK and non-SMK+abx) or 19 mice (SMK+abx). Results pooled from two independent experiments; day 35: one-way ANOVA and Sidak. Inset shows iAUC, one-way ANOVA and Sidak. **c**, Weight change of HFD-fed mice during DMG supplementation. $n = 30$ (PBS) or 29 mice (DMG), pooled from 3 independent repeats; day 21: unpaired two-sided *t*-test. Inset shows iAUC, unpaired two-sided *t*-test. **d**, Caloric content per gram stool in HFD-fed mice during DMG supplementation. $n = 9$ (PBS) or 7 mice (DMG); unpaired two-sided *t*-test. **e**, Weight change during smoke exposure and cessation in HFD-fed mice given ACG supplementation from day 18. $n = 10$ (non-SMK, non-SMK+ACG and SMK+ACG) or 9 mice (SMK); day 49: one-way ANOVA and Sidak. Inset shows iAUC, one-way ANOVA and Sidak. **f**, Weight change during ACG supplementation of mice. Control (HFD only) and ACG (HFD+ACG), $n = 74$ mice per group, pooled from 6 independent repeats; day 35: unpaired two-sided *t*-test. Inset shows iAUC, unpaired two-sided *t*-test. **g**, Targeted mass spectrometry of tagged-ACG (D^2-ACG). HFD-fed mice were orally gavaged with D^{13}-choline sulfate, and fecal and plasma samples were collected after 4 h. $n = 8$ (non-SMK) or 9 mice (SMK, non-SMK+abx and SMK+abx); one-way ANOVA and Sidak. **h**, Plasma ACG in HFD-fed mice treated with PBS or DMG. $n = 9$ (PBS) or 10 mice (DMG); two-sided Mann–Whitney *U*-test. **i**, **j**, Effect of DMG (**i**) and ACG (**j**) supplementation in mice not exposed to smoke on cellular composition quantified by single-cell transcriptomics in epididymal-adipose tissues. Cell percentage within the immune population, $n = 4$, unpaired two-sided *t*-test. **k**, Top 25 genes correlated with weight in naive (Control) mice and mice treated with PBS, ACG or DMG. Gene expression shown as the *z*-score of pseudobulk transcripts per million in $Trem2^+$ macrophages, $n = 4$. Grey backgrounds indicate the cessation period. All data show the mean ± s.e.m. $^*P < 0.05$, $^{**}P < 0.01$, $^{***}P < 0.001$, $^{****}P < 0.0001$, exact *P* values are presented in Supplementary Table 1.

which is converted into choline predominantly by the microbiome. Metabolite assessment of its tagged products showed that fecal levels of tagged-choline (D^{13}-choline, Fig. 3c) and tagged-betaine (D^{11}-betaine, Fig. 3d) were increased in mice exposed to smoke compared with control mice, and antibiotic treatment abrogated these differences. Of note, tagged-betaine levels were also increased in the plasma of mice exposed to smoke (D^{11}-betaine, Fig. 3e), which indicates that there is probably a systemic influx of microbiome-derived betaine from the gut. This, in turn, leads to increased plasma levels of tagged, microbiome-derived DMG in mice exposed to smoke (D^8-DMG, Fig. 3f). Antibiotic treatment abrogated the cigarette-smoke-related increase in plasma tagged-DMG, which suggests that the smoke-related increase in systemic DMG depends on upstream microbiome-generated precursors.

Metabolite-driven weight regulation

We next determined the causal impacts of four out of the seven candidate metabolites (Supplementary Table 5) on SCWG. *N*-formylanthranilic

acid and trigonelline did not influence SCWG after continuous supplementation to antibiotic-treated HFD-fed mice exposed to smoke (Extended Data Fig. 9a, b). By contrast, continuous DMG supplementation to antibiotic-treated HFD-fed mice exposed to smoke restored SCWG despite microbiome depletion (Fig. 4a, LMM $P = 0.00447$; Extended Data Fig. 9c, experiment repeated three times). Moreover, mice fed a choline-deficient diet, thereby lacking the major dietary precursor of DMG, did not feature smoke-dependent increases in DMG (Extended Data Fig. 9d) despite increased BHMT expression in the liver induced by smoke exposure (Extended Data Fig. 9e). This, in turn, resulted in a lack of SCWG during cessation of smoke exposure (Fig. 4b; LMM $P = 0.001616$, pooled results from experiment repeated twice). Of note, HFD-fed mice not exposed to smoke and continuously administered with DMG (100 mg kg^{-1} day^{-1}; Extended Data Fig. 9f, Methods) for 14–49 days (Extended Data Fig. 9g for a 14-day supplementation period, LMM $P = 0.0018$; Fig. 4c for a 21-day supplementation period, LMM $P = 0.0017$ from a pool of 3 repeats; Extended Data Fig. 9h for a 49-day supplementation period, LMM $P = 4.78 \times 10^{-9}$ from a pool of 2 repeats) had a modestly increased weight gain rate that was accompanied by unaltered metabolic features (Extended Data Fig. 9i–m). Moreover, these mice had lower levels of residual fecal calories than vehicle-treated mice, which probably reflects a higher gastrointestinal energy harvest capacity (Fig. 4d).

Another metabolite associated with SCWG (Supplementary Table 5) is ACG, which is a derivative of the amino acid glycine. Significantly lower plasma levels of ACG were observed among HFD-fed mice exposed to smoke and to smoke exposure cessation. ACG levels increased to those of no smoke exposure levels after antibiotic-mediated microbiome depletion (Extended Data Fig. 10a). To test the effects of ACG on SCWG, HFD-fed mice were administered ACG incorporated into the diet (given its low water solubility, this was HFD containing 7,500 mg kg^{-1} *N*-acetylglycine). Bomb calorimetry analysis confirmed that both the HFD and the ACG+HFD had comparable caloric contents, which were significantly higher than NC (Extended Data Fig. 10b), and that food-incorporated ACG supplementation induced a systemic increase in ACG levels (Extended Data Fig. 10c). In the SCWG model, ACG supplementation to HFD-fed mice exposed to smoke ameliorated SCWG (Fig. 4e; LMM $P = 2.06 \times 10^{-5}$, experiment repeated twice). Of note, HFD-fed mice supplemented with ACG for 35 days (and not exposed to smoke) had a significantly lower weight gain rate compared with HFD-fed control mice (Fig. 4f (LMM $P = 1.04 \times 10^{-21}$, pooled results from experiment repeated 6 times), and an additional repetition terminated after 15 days of ACG supplementation, Extended Data Fig. 10d (LMM $P = 0.006$)). These ACG-mediated weight-reducing effects were coupled with improvements in glucose tolerance (Extended Data Fig. 10e), increased plasma albumin, reduced plasma triglycerides, and improved alanine aminotransferase activity (Extended Data Fig. 10f). In ACG-supplemented mice, caloric intake was slightly increased (Extended Data Fig. 10g), and locomotion, respiratory exchange ratio and energy expenditure were similar to non-ACG-supplemented control mice (Extended Data Fig. 10h–j). Interestingly, the microbiome-dependent increase in systemic D^8-DMG levels noted in HFD-fed mice exposed to smoke following administration of D^{13}-choline sulfate (Fig. 3f) was accompanied by a concomitant microbiome-dependent systemic reduction in tagged-ACG (D^2-ACG) levels, which was abrogated by treatment with antibiotics (Fig. 4g). Similarly, DMG supplementation to HFD-fed mice not exposed to smoke induced a reduction in plasma ACG (Fig. 4h), whereas ACG supplementation did not affect systemic DMG levels (Extended Data Fig. 10k). These results suggest that a microbiome-dependent interconnection exists between the DMG and ACG biosynthetic pathways, which merit further studies.

Next, we performed a single-cell transcriptomics analysis of epididymal-adipose immune cells in HFD-fed mice after DMG and ACG supplementation (Extended Data Fig. 11a–d, Supplementary Table 6). DMG treatment led to an increase in adipose tissue $Ly6C^+$ monocytes, which have been shown to contribute to an obesity-associated pro-inflammatory programme[19] (Fig. 4i). Treatment with ACG led to lower levels of $Trem2^+$ macrophages, which have been correlated with adiposity and weight gain in mice and humans[20] (Fig. 4j). Similarly, multiple adipose-tissue genes, mostly related to obesity and associated pathways, including immune response, lysosome function, tissue remodelling, extracellular matrix, removal of dead cells and angiogenesis[21–23], exhibited opposite differential expression patterns in DMG- and ACG-supplemented mice (Extended Data Fig. 12a). These genes included those expressed in $Trem2^+$ adipose tissue macrophages, such as *Rcn3*, *Tspan4* and *Pla2g7* (Fig. 4k). Future studies will define the molecular nature and mechanisms of action of these metabolites on adipose tissue immunity, as well as the effects of other identified cigarette-smoke-related metabolites on such features.

Metabolite alterations in humans who smoke

Finally, we utilized baseline samples of an unrelated human clinical trial to characterize the microbiome profile of a small cross-sectional age- and sex-matched cohort of 96 participants (Methods, Extended Data Fig. 13a, Supplementary Table 7). To study the differences between those who actively smoke and those who do not smoke, in light of the results from the mouse model, we constructed a metagenomic reference catalogue of bacterial genomes assembled from metagenomes of our mouse models (Methods, Supplementary Table 7) and featuring a potential to drive the SCWG effect. Compared with participants who do not smoke ($n = 40$), fecal microbiomes from participants who smoke ($n = 20$) had a distinct taxonomic composition (Extended Data Fig. 13b, c, Supplementary Table 7) and KEGG Orthology composition (KO, Extended Data Fig. 13d, e, Supplementary Table 7). A binary classifier (Methods) successfully discriminated participants who smoke from those who do not smoke based on microbiome taxonomic composition (Extended Data Fig. 13f). Participants who smoke had elevated levels of plasma choline, betaine and DMG (do not smoke = 62, do smoke = 34; Extended Data Fig. 13g–i), similar to the results from the mouse model. These preliminary findings merit future larger-scale controlled studies.

Discussion

Our results mechanistically highlight the intensive cooperation prevailing between microbial and host components of the holobiont in driving SCWG. Together, they contribute to an increase in conversion of dietary choline to bioactive DMG, to a reduction in bioactive ACG and, possibly, to effects mediated by other cigarette-smoke-altered metabolites. A similar co-evolutionary concept was suggested for the carnitine–trimethylamine–trimethylamine-*N*-oxide pathway in the context of atherosclerosis[24]. We hypothesize that the gradual development of dysbiosis and associated metabolite alterations during smoking, including excessive production of DMG and related suppression of ACG, may serve as a feedback loop to the dominant non-microbiome-dependent anorexia that characterizes active cigarette smoking. Following smoking cessation, the anorexic signals rapidly dissipate while the obesogenic 'smoking microbiome' configuration and accumulated metabolites are slow to reverse. This can ultimately lead to SCWG.

As smoking is a voluntary human behaviour that is not possible to replicate in mice, it is unlikely that the model described here fully explains the human SCWG phenotype, which merits further large-scale studies. With these limitations notwithstanding, our results provide a proof of concept for a previously unappreciated microbiome involvement in SCWG and suggest that targeted dietary, microbial and postbiotic therapy may be utilized in attenuating SCWG and optimizing long-term abstinence success. Intriguingly, our postbiotic metabolite interventions resulted in phenotypic weight-related effects in mice even in the absence of exposure to cigarette smoke. The potential utility of identified metabolites as human interventions, in the smoking and non-smoking setting, merits further studies.

Online content

Any methods, additional references, Nature Research reporting summaries, source data, extended data, supplementary information, acknowledgements, peer review information; details of author contributions and competing interests; and statements of data and code availability are available at https://doi.org/10.1038/s41586-021-04194-8.

1. Centers for Disease Control and Prevention (CDC). Vital signs: current cigarette smoking among adults aged ≥18 years with mental illness—United States, 2009–2011. *MMWR Morb. Mortal Wkly Rep.* **62**, 81–87 (2013).
2. Centers for Disease Control and Prevention (CDC). Quitting smoking among adults—United States, 2001–2010. *MMWR Morb. Mortal Wkly Rep.* **60**, 1513–1519 (2011).
3. Harris, K. K., Zopey, M. & Friedman, T. C. Metabolic effects of smoking cessation. *Nat. Rev. Endocrinol.* **12**, 299–308 (2016).
4. Aubin, H. J., Farley, A., Lycett, D., Lahmek, P. & Aveyard, P. Weight gain in smokers after quitting cigarettes: meta-analysis. *BMJ* **345**, e4439 (2012).
5. Biedermann, L. et al. Smoking cessation induces profound changes in the composition of the intestinal microbiota in humans. *PLoS ONE* **8**, e59260 (2013).
6. Rodin, J. Weight change following smoking cessation: the role of food intake and exercise. *Addict. Behav.* **12**, 303–317 (1987).
7. Hankey, C. & Leslie, W. Obesity: is weight gain after smoking cessation an important concern? *Nat. Rev. Endocrinol.* **8**, 630–632 (2012).
8. Biedermann, L. et al. Smoking cessation alters intestinal microbiota: insights from quantitative investigations on human fecal samples using FISH. *Inflamm. Bowel Dis.* **20**, 1496–1501 (2014).
9. Lee, S. H. et al. Association between cigarette smoking status and composition of gut microbiota: population-based cross-sectional study. *J. Clin. Med.* **7**, 282 (2018).
10. Lim, M. Y. et al. Analysis of the association between host genetics, smoking, and sputum microbiota in healthy humans. *Sci. Rep.* **6**, 23745 (2016).
11. Russell, M. A., Wilson, C., Patel, U. A., Feyerabend, C. & Cole, P. V. Plasma nicotine levels after smoking cigarettes with high, medium, and low nicotine yields. *BMJ* **2**, 414–416 (1975).
12. Benowitz, N. L. & Jacob, P. 3rd Daily intake of nicotine during cigarette smoking. *Clin. Pharmacol. Ther.* **35**, 499–504 (1984).
13. Bush, T., Lovejoy, J. C., Deprey, M. & Carpenter, K. M. The effect of tobacco cessation on weight gain, obesity, and diabetes risk. *Obesity* **24**, 1834–1841 (2016).
14. Graff-Iversen, S., Hewitt, S., Forsen, L., Grotvedt, L. & Ariansen, I. Associations of tobacco smoking with body mass distribution; a population-based study of 65,875 men and women in midlife. *BMC Public Health* **19**, 1439 (2019).
15. Crooks, P. A., Bardo, M. T. & Dwoskin, L. P. Nicotinic receptor antagonists as treatments for nicotine abuse. *Adv. Pharmacol.* **69**, 513–551 (2014).
16. Turnbaugh, P. J. et al. An obesity-associated gut microbiome with increased capacity for energy harvest. *Nature* **444**, 1027–1031 (2006).
17. Langille, M. G. et al. Predictive functional profiling of microbial communities using 16S rRNA marker gene sequences. *Nat. Biotechnol.* **31**, 814–821 (2013).
18. Teng, Y. W., Mehedint, M. G., Garrow, T. A. & Zeisel, S. H. Deletion of betaine-homocysteine *S*-methyltransferase in mice perturbs choline and 1-carbon metabolism, resulting in fatty liver and hepatocellular carcinomas. *J. Biol. Chem.* **286**, 36258–36267 (2011).
19. Hill, D. A. et al. Distinct macrophage populations direct inflammatory versus physiological changes in adipose tissue. *Proc. Natl Acad. Sci. USA* **115**, E5096–E5105 (2018).
20. Jaitin, D. A. et al. Lipid-associated macrophages control metabolic homeostasis in a Trem2-dependent manner. *Cell* **178**, 686–698.e14 (2019).
21. Coats, B. R. et al. Metabolically activated adipose tissue macrophages perform detrimental and beneficial functions during diet-induced obesity. *Cell Rep.* **20**, 3149–3161 (2017).
22. Crewe, C., An, Y. A. & Scherer, P. E. The ominous triad of adipose tissue dysfunction: inflammation, fibrosis, and impaired angiogenesis. *J. Clin. Invest.* **127**, 74–82 (2017).
23. Flaherty, S. E. 3rd et al. A lipase-independent pathway of lipid release and immune modulation by adipocytes. *Science* **363**, 989–993 (2019).
24. Koeth, R. A. et al. Intestinal microbiota metabolism of L-carnitine, a nutrient in red meat, promotes atherosclerosis. *Nat. Med.* **19**, 576–585 (2013).

Methods

Mice

Eight-week-old C57BL/6J male mice were purchased from Harlan (or The Jackson Laboratory, specifically for one experiment). All mice were maintained in the animal facility of the Weizmann Institute and acclimated for 2 weeks before the initiation of experiments and fed on NC. All mice in all cigarette-smoke exposure experiments, unless otherwise specified, consumed a HFD (60% kcal from fat; Research Diets, D12492) 3 days before the experimental starting point. The choline-deficient diet (HFD containing 60% kcal from fat without added choline; Research Diets, D05010403) was also given 3 days before the start of the experiment. In experiments using ACG (the above HFD (Research Diet D12492) pellets prepared after supplementation with 7,500 mg kg^{-1} *N*-acetylglycine), mice were initially fed with HFD, which was then replaced with ACG+HFD 3 days before cessation of smoke exposure and during the entire cessation period. In all experiments, mice were randomly assigned to each group based on their weight to create weight-matched groups and to eliminate weight differences at the beginning of the experiments. Two weeks before the initiation of the experiment, antibiotic-treated groups received a combination of vancomycin (0.5 g l^{-1}), ampicillin (1 g l^{-1}), neomycin (1 g l^{-1}) and metronidazole (1 g l^{-1}) ad libitum in their drinking water. The mice were weighed every week to calculate the percent weight change induction by the HFD or the NC. Lean and fat mass were determined by nuclear magnetic resonance using a Bruker minispec LF50/mq7.5 MHz live mouse analyser. All experimental procedures were approved by the local Institutional Animal Care and UseCommittee 09890119-3 and 01480221-1.

Cigarette-smoke exposure

An automated cigarette smoking machine (model TE-10, Teague Enterprises) was used to generate the cigarette smoke exposure model in mice. Mice were exposed twice a day to cigarette smoke, 5 days per week for 3 weeks. During the acute smoke exposure period, mice underwent cigarette smoke exposure twice a day for 144 min with one rest interval of 120 min. Cigarette-smoke-exposed mice were placed in a whole-body exposure chamber attached to the smoking apparatus, the mixing chamber and the air pump. Mainstream (which simulates active smoking) and side-stream (which simulates passive smoking) cigarette smoke were mixed and allowed to flow through the chamber. Kentucky (Tobacco and Health Research Institute, University of Kentucky) 3R4F reference cigarettes (or 2R5F for the low-nicotine cigarettes experiment) were constantly burning and smoked using the Federal Trade Commission method, which consists of 2-s puffs of 35 cc each at 1-min intervals. Each cigarette was smoked for 9 min. The chamber flow rate and the number of cigarettes smoked in parallel were adjusted to reach 150 mg m^{-3} intermediate levels of smoke inside the whole-body exposure chamber. Smoke levels were measured at least twice a day. Cigarettes were stored at 4 °C before use. At least 48 h before use, the cigarettes were placed in a closed chamber along with a solution of glycerin/water (mixed in a ratio of 0.76:0.26) to establish a relative humidity of 60%.

Ten-week-old C57BL/6J male mice were subjected to cigarette-smoke-exposure sessions twice a day in a whole-body exposure chamber. In total, 64 research cigarettes per day per mouse were consumed for a period of 3 weeks. Using this regimen, cotinine (the major breakdown product of nicotine) plasma levels were comparable to those measured in humans who are active cigarette smokers[25]. To induce obesogenic conditions favouring the induction of SCWG, all mice in all cigarette-smoke exposure experiments, unless otherwise specified, consumed HFD from 3 days before the start of cigarette-smoke exposure for the duration of the experiment. To control for housing-related confounders, littermate controls were subjected to the same confined smoking chamber environment, without smoke exposure, in all experiments (termed Non-SMK or NS). After 3 weeks of smoke exposure, exposure was ceased in one of the smoke-exposed groups ('cessation' group), whereas it actively continued in 'continuous smoke exposure' group (Extended Data Fig. 1a). Mice that did not complete the acute smoke exposure or cessation periods were excluded from the incremental area under the curve (iAUC) calculations and its related statistical test for this period. For key experiments, individual repeats were performed by two different investigators.

Bomb calorimetry

Fecal samples were collected and stored at −80 °C. Before use, samples were dried using a FreeZone 4.5-litre cascade benchtop freeze dry system (Labconco) for 24 h. Gross energy content was measured using a water handling system (6510) and a bomb calorimeter (6200), both from Parr Instrument. The calorimeter energy equivalent factor was determined using benzoic acid standards. For each sample, the number of calories was normalized to its stool weight.

Metabolic cages

Metabolic cages (PhenoMaster system, TSE-Systems) were used to continuously measure food and liquid intake, energy expenditure, locomotor activity and respiratory exchange ratio. The system consists of a combination of sensitive feeding sensors for automated measurements, gas calorimetry to calculate the energy expenditure of each mouse, and a photobeam-based activity monitoring system for ambulatory movements. Mice were acclimated to metabolic cage accommodation in parallel to the ongoing experiment without impairing its course or delaying the designated experimental milestones. Training included three separate sessions of 4 h each, after which mice were returned to their original cages. To account for increased animal stress as a consequence of cage transfer and single-housing, we excluded the data acquired in the first 24 h. Randomly selected mice from the smoke-exposure experiments were transferred into the metabolic cages immediately after the last exposure to cigarette smoke.

Plasma samples

Mice were anaesthetized by an intraperitoneal injection of ketamine (100 mg kg^{-1}) and xylazine (10 mg kg^{-1}). Blood was collected by retro-orbital sinus puncture through the medial canthus of the eye using glass capillaries. Blood samples were collected into heparin-coated tubes and kept on ice. Samples were then centrifuged for 15 min at 10,000*g* at 4 °C. Plasma was collected and stored in −80 °C until use. Plasma levels of alanine aminotransferase, aspartate aminotransferase, cholesterol, ammonia and triglycerides were obtained using a Roche Cobas 111 serum analyser according to the manufacturer's instructions.

Fecal microbiome transplantation

C57BL/6J and SW GF mice were bred in the Weizmann Institute's GF facility and routinely monitored for sterility. For the fecal transplantation experiment, 200 mg of stool per recipient (from frozen glycerol donor mouse pellets) was suspended in sterile PBS ($-Ca^{2+}$, $-Mg^{2+}$), vortexed until dissolved and allowed to precipitate for 10 min. Recipient mice were administered 200 µl of the supernatant solution by oral gavage. After transplantation, all mice were housed in sterilized/autoclaved gnotobiotic iso-cages to minimize unwanted exogenous colonization. In the FMT set of experiments, the weight change was calculated as the relative change from the mean weight of each cage at day 0. The time-series analysis of weight change was performed using lmer (linear mixed effect model and lmer test, see 'Statistical analysis' section) accounting for the time, the source of fecal donation (smoke exposure versus no smoke exposure) and interaction of these factors. Cage identifiers were used as a source of random variation, which resulted in the following equation: weight change = time × donation + (1 | cage). For pools of several experimental repeats, the random effect component in the formula was (1 | batch:cage) where batch denotes the experimental repeat.

16S rDNA sequencing

Fresh fecal pellets were aseptically collected into sterile tubes, snap-frozen in liquid nitrogen and stored at −80 °C. DNA was isolated from fecal samples using a PowerMag Soil DNA isolation kit (Qiagen) optimized for the Tecan automated platform. PCR amplification was performed on the entire V4 region of the 16S rDNA gene using the 515F (GTGCCAGCMGCCGCGGTAA)/806R (GGACTACHVGGGTWTCTAAT) primers. Sequencing of these amplicons was performed on an Illumina MiSeq sequencer using 2 × 250-bp paired-end reads.

16S rDNA analysis

MiSeq (Illumina) fastq files were analysed using Qiime2 (v.2018.4.0). Using the demux-emp-paired plugin and the barcode mapping file, the reads were demultiplexed and assigned to their corresponding sample. De-noising and amplicon sequencing variants (ASV) tables were constructed using DADA2 plugin via command dada2-denoise-paired. Samples that did not reach the established sequencing depths (44,946, 50,173 and 30,014 reads for the smoke exposure, intraperitoneal nicotine and oral nicotine experiments, respectively) were excluded from further analysis. ASVs were assigned with taxonomic annotations by applying the feature-classifier plugin (classify-sklearn) to our representative sequences and using a naive Bayes taxonomic classifier downloaded from Qiime's data-resources page. Functional composition was established from 16S rDNA using PICRUSt2 plugin for Qiime2 (v.2019.7.0)[26].

Metabolite candidate assessment

For each plasma metabolite, a LMM accounting for smoke exposure, antibiotic treatment and time was fitted to identify patterns that paralleled the SCWG phenotype in the mouse groups exposed/not exposed to smoke and their respective antibiotic-treated groups (see 'Statistical analysis' section). Collectively, 41 metabolites (out of 627 annotated plasma metabolites) were significantly affected by smoke exposure, antibiotic treatment and their interactions (Extended Data Fig. 8c). A post hoc test (Sidak's) further refined the candidate metabolite search according to the following criteria for the interactions: (1) significant differential expression between mice exposed to smoke and not exposed to smoke; (2) significant differential expression between mice exposed to smoke and antibiotic-treated mice exposed to smoke; (3) non-significant differential expression between antibiotic-treated and non-treated mice not exposed to smoke; and (4) non-significant differential expression between antibiotic-treated mice not exposed to smoke and antibiotic-treated mice exposed to smoke.

Shotgun metagenomic sequencing

Illumina libraries were prepared using a Nextera DNA Library Prep kit (Illumina, FC-121-1031) according to the manufacturer's protocol and sequenced on an Illumina NextSeq platform with a read length of 75 bp (single-end) for all samples except for Fig. 2a and for the inset of Fig. 2f and Extended Data Fig. 6b, for which paired-end sequenced with a read length of 75 bp was used.

Murine metagenomic analysis

Bcl2fastq (v2.17.1.14) was used to convert the raw output bcl files to fastq files. Reads were then QC trimmed using Trimmomatic (v.0.39)[27]. Bowtie2 (v.2.3.5.1) alignment against the mm10 host reference was performed (very sensitive preset), and reads mapping to the host reference were removed. For the specific pathogen-free (SPF) experimental setup, the read files of all samples were subsampled to a uniform depth of 11.4 million reads per sample (5.7 per mate). Fecal transplant experiments were single-end sequenced in the same platform and rarefied to 3 million reads. Subsampling of reads was done using seqtk (v.1.2). Taxonomic annotation of short reads was performed using Kraken2 (v.2.0.8)[28] mapping to GTDB reference (release 89) followed by the execution of Bracken (v.2.5). Functional annotations were done using diamond (v.0.9.24)[29] through a translated search (blastx) of the short reads against a reference database that included all EC-annotated entries of bacterial organisms found in UniProt. Statistical analysis of count data was conducted using DESeq2. Differential relative abundance tests for compositional data were performed using Mann–Whitney *U*-tests. All heatmaps present features that were the top-ranking contributors to a partial least-squares discrimination model.

Human cohort metagenomic analysis

Annotation of the human metagenomes was done using a metagenome-assembled genomes (MAGs) reference catalogue, assembled using metagenomes of the murine fecal transplant experiment (Fig. 2f, Extended Data Fig. 6b, insets), which were paired end and sequenced to a mean depth of 20.4 M±1.48 M (s.d.) reads per mate (40.8 M ± 2.96 s.d. overall). A KEGG-annotated gene catalogue was constructed out of the MAGs found using Anvi'o software, following the methodology as described[30]. Specifically, a co-assembly of contigs was created for the union of all reads from each group in the experiment using MegaHit[31]. For each contigs database (db), HMMER[32] was then used to identify bacterial and archaeal genes. Taxonomic identification was done using Centrifuge[33]. Each sample was then mapped to the scaffolds of its group using bowtie2, and mapping results were profiled by coverage and detection estimation of each scaffold. Profiles of the same group were then merged and contigs therein binned using CONCOCT[34]. After manual curation of the bins, a recommended step in the Anvi'o pipeline, MAGs were defined as bins with >70% completion in <10% redundancy. Dereplication of the MAGs from all profiles was done using fastANI[35] (97% similarity and *k*-mer size of 10). Gene calls with KEGG annotations were extracted from the non-redundant MAGs collection to form the gene catalogue. Then single-end, shotgun metagenomic samples from the human cohort were pre-processed in a similar way to the murine metagenomic data, with the exception of using reference hg19 for removal of host reads. Reads were then subsampled to an even depth of 8 million reads, and samples of shallower sequencing depth were omitted from the analysis, which resulted in a cohort of 60 human participants. Finally, metagenomic profiles of the human samples were obtained by mapping the reads against the gene catalogue described above using bowtie2. A binary classifier was trained by fitting a GradientBoosting classifier on top of partial least-squares regression (both implemented in scikit-learn Python package, v.0.20.0) with default hyperparameters. The receiver operating characteristic curve was evaluated by executing stratified *k*-fold iterations for six different splits.

Single-cell RNA sequencing

Epididymal-adipose tissue from controls and treated (with DMG and ACG) mice ($n = 4$ per group) was dissected and placed in 5 ml of DMEM (without phenol red, 4,500 mg l^{-1} glucose) at room temperature and disintegrated by chopping with sterile scissors. Subsequently, 0.2 g ml^{-1} of collagenase II (Sigma-Aldrich, C6885) was added and samples were incubated for 20 min at 37 °C with shaking. Subsequently, 5 ml of cold DMEM was added to each sample and filtered through a 250-µm mesh. Samples were centrifuged at room temperature for 5 min at 300*g* without breaks and with slow acceleration. The pellets containing immune cells were recovered, resuspended in 0.5 ml ACK buffer (Gibco, A1049201), and incubated for 1 min. Then, 14 ml of PBS was added, and cells were collected by centrifugation at 500*g* for 10 min. Pellets were resuspended in PBS with 0.04% BSA, filtered through a 40-µm mesh, counted and loaded onto a Chromium 3′ RNA v3.1 chip (10X Genomics) aiming for 6,000 cells per sample. Libraries were prepared according to the manufacturer's instructions and sequenced on a Novaseq6000 (R2 89bp).

Single-cell RNA-sequencing data analysis

Data were demultiplexed, mapped and unique transcripts were counted using the Cell Ranger pipeline (v.6.0.0) and GRCm38.p4 mouse genome. A total of 16 samples were combined using aggr with the default

downsampling normalization disabled. Raw count matrix was imported into R for further analysis. Cells with fewer than 600 transcripts and with more than 20% reads mapping to the mitochondrial genomes were filtered, as well as genes detected in fewer than 3 cells. Data were normalized and scaled using Seurat package (v.3.2.3)[36]. Next, 2,000 of the most variable genes were identified using the 'vst' method and FindVariableFeatures function, and dimensionality was reduced using principal component analysis. The first 30 dimensions were used to construct a shared nearest neighbour graph based on which clusters were identified. Clusters containing immune cells were identified by the expression of *Ptprc*, subsetted and reclustered in the same manner as described above. Clusters containing doublets were removed from the analysis. Remaining cells were divided into the following categories: (1) T cells and innate lymphoid cells (ILCs); (2) macrophages and dendritic cells (subset 2); and (3) remaining cells (which were clustered again and annotated based on previously published data[20,37]).

Differential expression was performed by calculating pseudobulk transcriptomes for each cluster and each condition using DESeq2 (v.1.30.0)[38]. Gene Ontology analysis was performed using differentially expressed genes (adjusted *P* value of < 0.05) and gprofiler2 package (v.0.2.0)[39] with the function ordered_query =T.

Quantitative PCR

DNA templates were diluted to a final amount of 1 ng per reaction. Amplifications were performed with the following primer sets: *BHMT* forward, 5′-GCCACCGGCTTCAGAAAAA-3′; *BHMT* reverse, 5′- CCGGAAGCTATTCGCAGATT-3′. *HPRT* forward, 5′-TCAGTCAACGGGGGACATAAA-3′; and *HPRT* reverse, 5′-GGGGCTGTACTGCTTAACCAG-3′. Fast SYBR Green Master Mix (ThermoFisher) was used in duplicates. Amplification conditions were as follows: denaturation at 95 °C for 20 s, followed by 40 cycles of denaturation at 95 °C for 1 s; annealing at 60 °C for 20 s followed by melting curve. Duplicates with >1 cycle difference were excluded from the analysis. Data were analysed using the ΔCt method.

Targeted metabolomics

d4-nicotinamide and ^{13}C6-arginine (10 ng ml^{-1} and 200 ng ml^{-1}, respectively; Cambridge Isotope Laboratories) were added as internal standards. Liquid chromatography with tandem mass spectrometry (LC–MS/MS) analysis was performed on an Acquity UPLC system and triple quadrupole Xevo TQ-S (both Waters). TargetLynx (Waters) was applied for quantitation based on standard curves. Stool samples were weighed into 2-ml safe-lock Eppendorf tubes, and 300 µl of 70% ethanol in double-distilled water was added. Samples were homogenized using a bead beater with metal balls. Plasma samples (30 µl) were mixed with 90 µl of 70% acetonitrile. The extracts were centrifuged and filtered through PTFE 0.2-µm filter vials (Thompson) for analysis of DMG, trimethylglycine and choline. For analysis of nicotine and cotinine, samples were dried in a speed vac to remove the methanol before drying was completed in a lyophilizer, then re-dissolved in 100 µl of 20% ethanol, centrifuged and filtered through PVDF 0.2-µm filters (Millex-GV, Millipore). Metabolites levels below 0.001 ng ml^{-1}were defined as 0.001. Stool metabolites (ng ml^{-1}) were normalized per mg of stool.

Nicotine and cotinine. The following LC parameters were used: acquity BEH C8 column (2.1 × 100 mm, 1.7 µm; Waters) at 30 °C. Gradient conditions of mobile phases A (10 mM ammonium formate, pH 3.0) and B (acetonitrile) were as follows: 0 min, 5% B; 2.5 min, 45% B; 2.8 min, 100% B; 3.3 min, 5% B; 5 min, 5% B. The injection volume was 1.0 µl and the flow rate was 0.2 ml min^{-1}. The following MS/MS parameters were used: electrospray ionization in positive-ion mode, desolvation temperature, 400 °C; desolvation gas flow, 700 l h^{-1}; cone gas flow, 150 l h^{-1}; nebulizer pressure, 7 Bar; capillary voltage, 0.5 kV, cone voltage 25 V. The MRM transitions were as follows: nicotine: 163.1 > 130.1 and 163.1 > 132.1, collision energy (CE) 16 and 12 V, respectively; cotinine: 177.1 > 80.0 and 177.1 > 98.1, CE 18 for both; d4-nicotinamide: 127 > 81 and 127 > 84, CE 19 and 17 V, respectively, with argon 0.10 mg min^{-1} as the collision gas.

DMG, betaine, ACG and choline. The following LC parameters were used: Atlantis Premier BEH C18 AX (2.1 × 100 mm, 1.7 µm; Waters) at 25 °C. Gradient conditions of mobile phases A (0.2% formic acid in water) and B (0.2% formic acid in acetonitrile) were as follows: 0.1% B for 2 min; increase to 100% B for 4 min; hold at 100% B during 1 min; back to 0.1% B for 1 min, then equilibration 5 min. The injection volume was 1.0 µl and the flow rate was 0.1 ml min^{-1}. The following MS/MS parameters were used: electrospray ionization in positive-ion mode, desolvation temperature 400 °C; desolvation gas flow 600 l h^{-1}; cone gas flow 150 l h^{-1}; nebulizer pressure 7 Bar; capillary voltage, 0.6 kV, cone voltage 22 V.

The MRM transitions were as follows: DMG: 104.0 > 58.1, CE 11 V; betaine: 118.1 > 59.2, CE 15 V; choline: 104.2 > 60.2, CE 14 V; ACG: 117.8 > 75.8, CE 7 V, ^{13}C6-arginine: 181.1 > 61.1 and 181.1 > 74.2 CE 16 V for both; d4-nicotinamide: as described above, with argon 0.10 mg min^{-1} as the collision gas.

Quantification of labelled D^{13}-choline sulfate products. D^{13}-choline sulfate products were analysed in a similar manner to the unlabelled samples described above. Aliquots of samples of each type were collected to form the pools. These pools were spiked with a non-labelled standard mix to build standard curves. No internal standards were used. The obtained standard curves were used for quantitation of corresponding labelled compounds assuming identical ionization of labelled and unlabelled metabolites.

The following MRM transitions were used: D^{13}-choline: 117.2 > 69.2, CE 14 V; D^{11}-betaine: 129.1 > 68.2, CE 15 V; D^{8}-DMG: 111.8 > 66.1, CE 11 V; D^{2}-ACG: 120.0 > 78.0, CE 7 V.

Untargeted metabolomics profiling

Fecal and blood samples were collected, snap-frozen in liquid nitrogen and stored at −80 °C until processing and analysis by Metabolon. In brief, samples were processed using an automated MicroLab STAR system (Hamilton). To remove protein, small molecules bound to protein or trapped in the precipitated protein matrix were dissociated, and to recover chemically diverse metabolites, proteins were precipitated with methanol. The resulting extract was divided into five fractions: ultra-pressure liquid chromatograph (UPLC)–MS/MS with positive-ion mode electrospray ionization; UPLC–MS/MS with negative-ion mode electrospray ionization; LC polar platform; gas chromatography (GC)–MS; and one sample was reserved for backup. Samples were placed briefly on a TurboVap (Zymark) to remove the organic solvent. For LC, the samples were stored overnight under nitrogen before preparation for analysis. For GC, each sample was dried under vacuum overnight before preparation for analysis. Data extraction and compound identification were as follows: raw data were extracted, peaks identified and QC was processed using Metabolon's hardware and software. Compounds were identified by comparison to library entries of purified standards or recurrent unknown entities.Values were first normalized for raw area counts. Values for each metabolite were then re-scaled to have a median of 1 (ignoring missing values). Missing values of each metabolite were imputed using the minimal observed value of that metabolite. This process results in a scaled, imputed dataset (SmD).

Metabolite supplementation

For in vivo supplementation, Alzet osmotic minipumps (model 2004) were used to infuse the compound at a rate of 0.25 µl h^{-1} for 28 days. The pumps were filled with 200 µl of the following metabolite: DMG (*N*,*N*-dimethylglycine, ≥99%, Sigma-Aldrich, 100 mg kg^{-1} day^{-1}); varenicline (varenicline tartrate, ≥98% HPLC, Sigma-Aldrich, 0.5 mg kg^{-1} day^{-1}); or trigonelline (trigonelline hydrochloride, analytical standard, Sigma-Aldrich, 70 mg kg^{-1} day^{-1}), diluted in PBS (−Ca^{2+}, −Mg^{2+}). Vehicle

control pumps contained an equivalent volume of PBS ($-Ca^{2+}$, $-Mg^{2+}$). Mice were anaesthetized by an intraperitoneal injection of ketamine (100 mg kg^{-1}) and xylazine (10 mg kg^{-1}) mixture; thereafter, the skin of the neck was shaved and sterilized with 70% ethanol. Then, a 1 cm incision was made in the skin, and the osmotic minipumps were subcutaneously inserted after minimal blunt dissection and placed above the right hind flank. The cut was then closed with sterile surgical clips and the mice were carefully monitored for any signs of stress, bleeding, pain or abnormal behaviour. For the in vivo administration of nicotine, mice were intraperitoneally injected with 0.15 mg ml^{-1} nicotine twice a day for 3 weeks. Formylanthranilic acid (Sigma-Aldrich) was dissolved in PBS ($-Ca^{2+}$, $-Mg^{2+}$) and added to drinking water for a final concentration of 0.35 mg ml^{-1}. For the administration of tagged- choline sulfate, mice were orally gavaged with 50 mg ml^{-1} of D^{13}-choline sulfate (Cambridge Isotope Laboratories). Four hours after administration, stool and plasma samples were collected.

Human trial

Data of the observational human cohort were obtained from baseline samples of an unrelated experiment, which was approved by the Weizmann Institute of Science Bioethics and Embryonic Stem Cell Research oversight committee (IRB approval number 170-2), registration number NCT03708939. The study has been completed and unpublished. Ninety-six healthy volunteers were recruited in Israel for this study between 2018 and 2020. Age- and body–mass index (BMI)-matched cohorts of participants who do not smoke ($n = 62$) and participants who are active smokers ($n = 34$) were utilized. Blood and stool samples were collected from the participants, and these samples were subjected to targeted mass spectrometry and metagenomic sequencing, respectively. All participants received financial compensation for their participation in the study. All participants fulfilled the following inclusion criteria: males and females aged 18–70 years; BMI < 28; and ability to provide informed consent. The following exclusion criteria were applied: (1) pregnancy or fertility treatments; (2) use of antibiotics or antifungals within 3 months before participation; (3) consumption of probiotics or non-nutritive sweeteners within 1 month before participation; (4) chronically active inflammatory, cardiovascular, infectious, endocrine or neoplastic disease within the 3 years before enrolment; (5) chronic gastrointestinal disorder, including inflammatory bowel disease and celiac disease or gastrointestinal surgery such as bariatric surgery; (6) neuropsychiatric disorder; (7) coagulation disorders; (8) pre-diagnosed type 1 or type 2 diabetes mellitus or treatment with anti-diabetic medications; (9) alcohol or substance abuse. Adherence to inclusion and exclusion criteria were validated by medical doctors.

Data integrity check

Figure and supplementary figure panels were checked for data integrity using the Proofig pipeline, https://www.proofig.com.

Statistical analysis

Statistical tests were performed using GraphPad Prism 9.2, Qiime2 plugins, R and python. Each treatment group consisted of at least two cages to control for cage effect. For pooled analysis of results from different independent repeats, all mice from the same experimental group were pooled and a new statistical comparison was made for the entire pooled experiment, as performed for the individual repeats. For comparisons between two groups, unpaired *t*-test or Mann–Whitney *U*-test was performed. Wilcoxon signed-rank tests were used to conduct paired comparisons. *F*-test or Kruskal–Wallis was used for comparisons of more than two groups. Correction of the multiple comparison tests Sidak, Tukey or Dunn. False discovery rate adjustment was performed using the Benjamini–Hochberg procedure. Nonparametric hypothesis testing methods were used for cases when the measured quantity could not be assumed to follow a normal distribution and failed to pass the Shapiro–Wilk normality test. For cases when missing values prevented the use of analysis of variance (ANOVA) with repeated measures, the analysis was done by fitting a LMM as implemented in GraphPad Prism 9.2. The LMM uses a compound symmetry covariance matrix and fits using restricted maximum likelihood. The weight change in the cessation of smoke-exposure experiments was modelled as follows: weight change (%) = time (days) × antibiotics (yes/no) × group (exposed/not exposed to smoke) + (1 | mouse). For the osmotic pump experiments: weight change = time × smoke exposure × pump (none, PBS, DMG, ACG) × antibiotics + (1 | mouse). For the analysis of pooled repetitions of the same experiment, to account for the variability between repetitions, the random effect component was formulated as (1 | batch:mouse) where batch is the experimental repetition identifier. Coefficient estimates, errors and *P* values obtained for the pooled experiments and separate repetitions therein are reported in Supplementary Table 1. Modelling the variation of metabolite levels in the metabolomics data was done using the following formulation: metabolite levels = time × antibiotics (yes/no) × group + (1 | mouse). Multivariate hypothesis testing for taxonomic and functional microbiome composition data was done using permutational analysis of variance (PERMANOVA) for comparisons between different time points of the same group. The permutations were stratified only to those shuffling labels of samples from the same mouse; in all cases, PERMANOVA was applied directly to the full (untruncated) distance/dissimilarity matrix. *P* values of <0.05 were considered significant. $^{*}P < 0.05$, $^{**}P < 0.01$, $^{***}P < 0.001$, $^{****}P < 0.0001$.

Reporting summary

Further information on research design is available in the Nature Research Reporting Summary linked to this paper.

Data availability

Raw metagenomic sequences and resolved MAGs are available at the European Nucleotide Archive under project accession number PRJEB40095. Single-cell RNA raw sequences are deposited in ArrayExpress with accession E-MTAB-10869. Metabolomic data are provided in Supplementary Table 4 and in the publicly accessible platform of Mendeley at https://doi.org/10.17632/539zh45tw2.1. Source data are provided with this paper.

25. Witschi, H., Espiritu, I., Dance, S. T. & Miller, M. S. A mouse lung tumor model of tobacco smoke carcinogenesis. *Toxicol. Sci.* **68**, 322–330 (2002).
26. Bolyen, E. et al. Reproducible, interactive, scalable and extensible microbiome data science using QIIME 2. *Nat. Biotechnol.* **37**, 852–857 (2019).
27. Bolger, A. M., Lohse, M. & Usadel, B. Trimmomatic: a flexible trimmer for Illumina sequence data. *Bioinformatics* **30**, 2114–2120 (2014).
28. Wood, D. E., Lu, J. & Langmead, B. Improved metagenomic analysis with Kraken 2. *Genome Biol.* **20**, 257 (2019).
29. Buchfink, B., Xie, C. & Huson, D. H. Fast and sensitive protein alignment using DIAMOND. *Nat. Methods* **12**, 59–60 (2015).
30. Delmont, T. O. et al. Nitrogen-fixing populations of Planctomycetes and Proteobacteria are abundant in surface ocean metagenomes. *Nat. Microbiol.* **3**, 804–813 (2018).
31. Li, D., Liu, C. M., Luo, R., Sadakane, K. & Lam, T. W. MEGAHIT: an ultra-fast single-node solution for large and complex metagenomics assembly via succinct de Bruijn graph. *Bioinformatics* **31**, 1674–1676 (2015).
32. Eddy, S. R. Accelerated Profile HMM Searches. *PLoS Comput. Biol.* **7**, e1002195 (2011).
33. Kim, D., Song, L., Breitwieser, F. P. & Salzberg, S. L. Centrifuge: rapid and sensitive classification of metagenomic sequences. *Genome Res.* **26**, 1721–1729 (2016).
34. Alneberg, J. et al. Binning metagenomic contigs by coverage and composition. *Nat. Methods* **11**, 1144–1146 (2014).
35. Jain, C., Rodriguez, R. L., Phillippy, A. M., Konstantinidis, K. T. & Aluru, S. High throughput ANI analysis of 90K prokaryotic genomes reveals clear species boundaries. *Nat. Commun.* **9**, 5114 (2018).
36. Stuart, T. et al. Comprehensive integration of single-cell data. *Cell* **177**, 1888-1902.e21 (2019).
37. Tabula Muris, C. et al. Single-cell transcriptomics of 20 mouse organs creates a *Tabula Muris*. *Nature* **562**, 367–372 (2018).
38. Love, M. I., Huber, W. & Anders, S. Moderated estimation of fold change and dispersion for RNA-seq data with DESeq2. *Genome Biol.* **15**, 550 (2014).
39. Raudvere, U. et al. g:Profiler: a web server for functional enrichment analysis and conversions of gene lists (2019 update). *Nucleic Acids Res.* **47**, W191–W198 (2019).

Acknowledgements We thank the members of the Elinav laboratory, Weizmann Institute of Science, and members of the DKFZ Cancer–Microbiome Division for insightful discussions; R. Alon, A. Bar-Shai and M. Hatzav for assistance with operation of the smoking machine; M. Eren for fruitful discussions and guidance on making the MAG reference catalogue; and C. Bar-Natan for care of the GF animals and animal work. A.A.K. is a recipient of EMBO Long Term Fellowship number 2016-1088 and the European Union's Horizon 2020 research and innovation programme under Marie Sklodowska–Curie grant agreement number 747114. M.T. is the Incumbent of the Carolito Stiftung Research Fellow Chair in Neurodegenerative Diseases. Y.K. is the incumbent of the Sarah and Rolando Uziel Research Associate Chair. H.S. is the incumbent of the Vera Rosenberg Schwartz Research Fellow Chair. E.E. is supported by the Leona M. and Harry B. Helmsley Charitable Trust, the Adelis Foundation, the Pearl Welinsky Merlo Scientific Progress Research Fund, the Park Avenue Charitable Fund, The Hanna and Dr. Ludwik Wallach Cancer Research Fund, the Daniel Morris Trust, The Wolfson Family Charitable Trust & The Wolfson Foundation, the Ben B. and Joyce E. Eisenberg Foundation, the White Rose International Foundation, the Estate of Malka Moskowitz, the Estate of Myron H. Ackerman, the Estate of Bernard Bishin for the WIS-Clalit Program, the Else Kroener Fresenius Foundation, the Jeanne and Joseph Nissim Center for Life Sciences Research, Aliza Moussaieff, Miel de Botton, the Vainboim Family, Alex Davidoff, the V. R. Schwartz Research Fellow Chair, the Swiss Society Institute for Cancer Prevention Research at the Weizmann Institute of Science, Rehovot, Israel and by grants funded by the European Research Council, the Israel Science Foundation, the Israel Ministry of Science and Technology, the Israel Ministry of Health, the Helmholtz Foundation, the Garvan Institute, the European Crohn's and Colitis Organization, the Deutsch–Israelische Projektkooperation, the IDSA Foundation, the Sagol Institute for Longevity Research Program, the Charlie Teo Foundation, and the Wellcome Trust. E.E. is the incumbent of the Sir Marc and Lady Tania Feldmann Professorial Chair, is a senior fellow of the Canadian Institute of Advanced Research (CIFAR), and is an international scholar of The Bill & Melinda Gates Foundation and Howard Hughes Medical Institute (HHMI).

Author contributions L.F. and U.M. contributed equally to the study. L.F. designed, performed, interpreted the experiments and wrote the manuscript. U.M. designed and headed all computational and analytical aspects related to this study. A.A.K., performed and analysed the single-cell transcriptomics analysis. M.D.-B., A. Leshem, S.I., S.H., H.K., D.K., A. Livne, C.M., S.M., N.A. and H.S. helped with experiments. Y.C., R.V.-M. and N.Z. assisted with data analysis. A. Brandis and T.M. performed the metabolomic experiments. Y.K. assisted with the metabolic cage experiments. M.T. assisted with the smoking-chamber experiments. N.S. and A.H. supervised all the GF experiments. J.S., A. Bukimer, S.E.-M. and A.M. designed and conducted the human trial, and assisted in the analysis of its results. H.S. and E.E. conceived the study, jointly supervised the participants, interpreted the experiments and wrote the manuscript.

Competing interests E.E. is the scientific founder of Daytwo & BiomX, and a consultant to HELLO INSIDE in topics unrelated to the subject of this work. L.F., U.M., A.A.K., M.D.-B., A. Leshem, S.I., Y.C., J.S., N.Z., C.M., S.M., N.A., R.V.-M., S.H., H.K., D.K., A. Livne, A. Brandis, S.E.-M., A.M., A. Bukimer, T.M., Y.K., M.T., N.S., A.H. and H.S. do not have any financial or non-financial competing interests. Weizmann Institute of Science is in the process of applying for a patent application covering weight modulatory effects of discovered microbes and metabolites that lists L.F., U.M. and E.E. as inventors.

Additional information

Supplementary information The online version contains supplementary material available at https://doi.org/10.1038/s41586-021-04194-8.

Correspondence and requests for materials should be addressed to Eran Elinav.

Peer review information *Nature* thanks the anonymous reviewer(s) for their contribution to the peer review of this work.

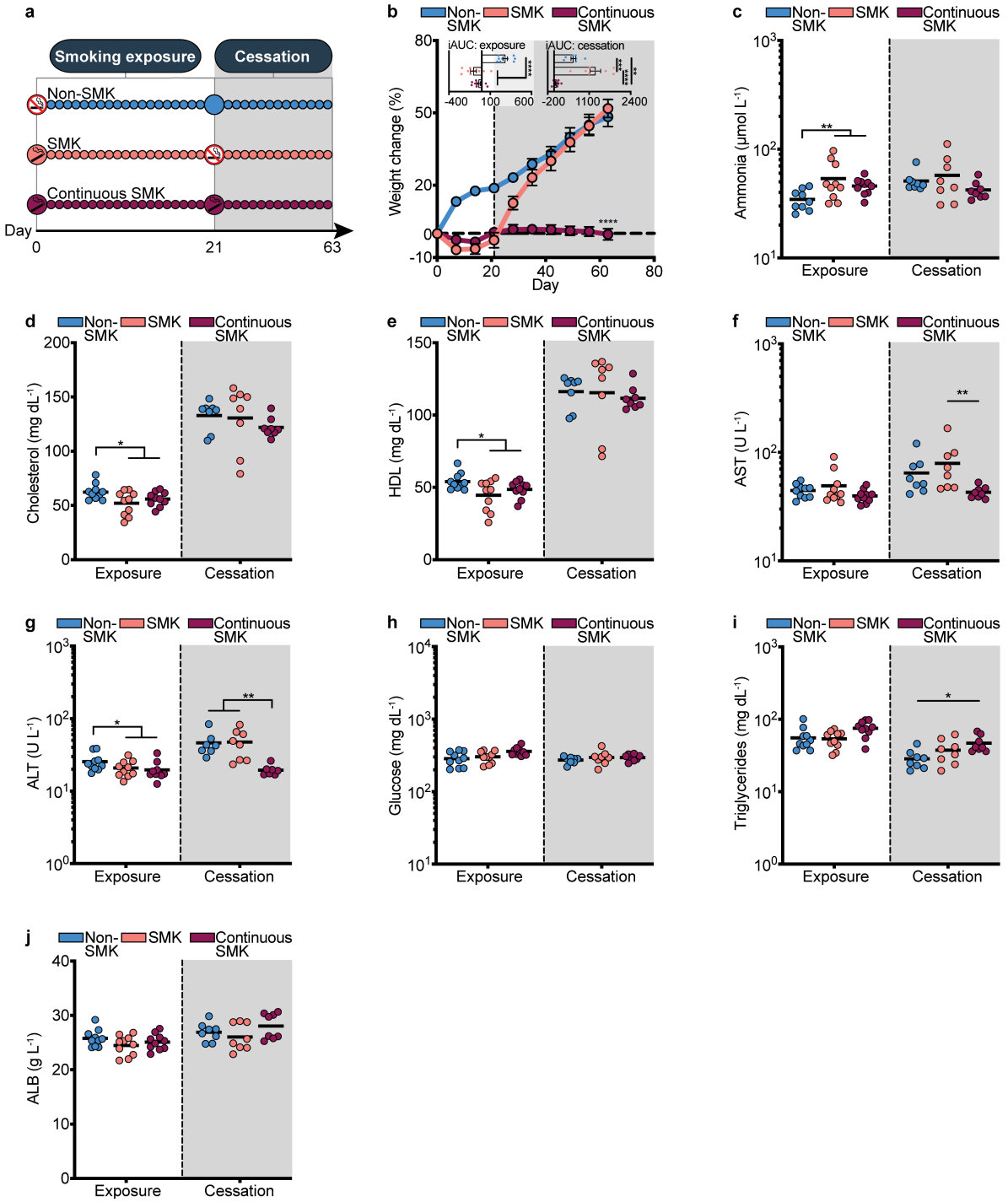

Extended Data Fig. 1 | See next page for caption.

Extended Data Fig. 1 | The smoking cessation mouse model. (a) Experimental scheme, HFD-fed mice. Mice not exposed to cigarette smoke (Non-SMK), mice exposed to smoke and cessation (SMK) and mice continuously exposed to smoke (continuous SMK). SMK group was exposed to cigarette smoke for 3 weeks, 5 days/week. Continuously smoke exposed group was exposed to cigarette-smoke throughout the duration of the experiment. **(b)** Weight change of HFD-fed mice during smoke exposure and following discontinuation of smoke exposure (cessation). Non-SMK, SMK and continuous SMK ($n = 10$), mean ± s.e.m.; day 63: one-way ANOVA and Tukey correction. Inset: iAUC of weight change at smoke exposure or cessation, one-way ANOVA and Tukey correction, mean ± s.e.m. **(c–e)** Ammonia **(c)**, cholesterol **(d)** and HDL **(e)** levels during smoke exposure and cessation: Non-SMK (at smoke exposure $n = 9$ for ammonia and $n = 10$ for d-e; at cessation $n = 8$ for all groups), SMK and continuous SMK (at smoke exposure $n = 10$, at cessation $n = 8$), mean values. Smoke exposure phase: two-sided Mann-Whitney *U*-test (**c**, **e**) or unpaired two-sided *t*-test (**d**); cessation: Kruskal-Wallis and Dunn's test. In the smoke exposure phase, SMK and continuous SMK were considered as one group. **(f–g)** Aspartate aminotransferase (AST, **f)** and alanine aminotransferase (ALT, **g)** levels during smoke exposure and cessation: Non-SMK, SMK, continuous SMK ($n = 10$ per group during smoke exposure; $n = 8$ per group during cessation); two-sided Mann-Whitney *U*- test for smoke exposure, Kruskal-Wallis and Dunn's test for cessation, mean values. **(h–j)** non-fasting glucose **(h)**, triglycerides **(i)** and albumin (ALB, **j)** levels during smoke exposure and cessation: Non-SMK, SMK and continuous SMK ($n = 10$ per group during smoke exposure, $n = 8$ per group during cessation). Glucose: unpaired two-sided *t*-test for smoke exposure and one-way ANOVA with Tukey correction for cessation; triglycerides and albumin: unpaired two-sided *t*-test for smoke exposure and Kruskal-Wallis and Dunn's test for cessation. Plasma samples were collected 21 days during smoke exposure and on day 63 during cessation, mean values. Grey backgrounds represent cessation period. *$P<0.05$; **$P<0.01$; ***$P<0.001$; ****$P<0.0001$, exact *P* values presented in Supplementary Table 1.

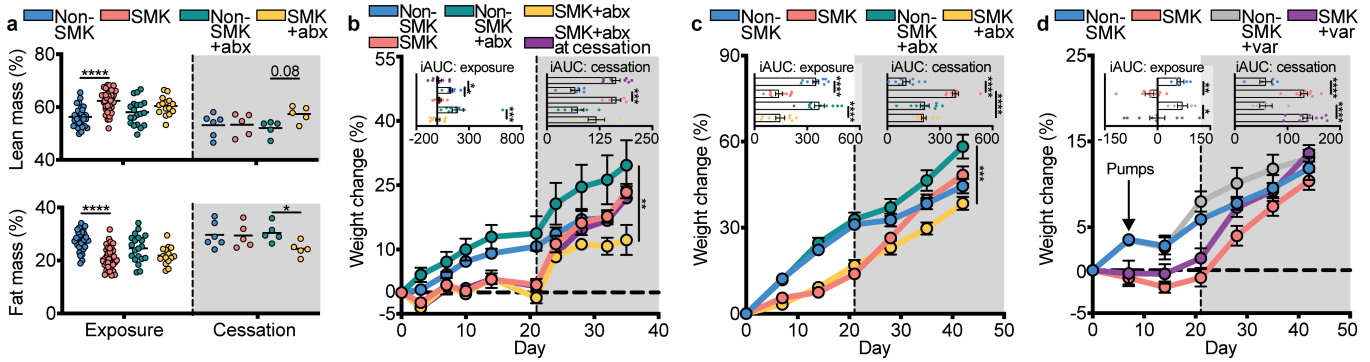

Extended Data Fig. 2 | Impact of microbiome depletion on SCWG. (a) Lean (top) and fat (bottom) mass during smoke exposure (day 19) and cessation (day 35). Non-SMK ($n = 30$ at smoke exposure, $n = 6$ at cessation), SMK ($n = 38$ at smoke exposure, $n = 5$ at cessation), Non-SMK+abx (at smoke exposure $n = 20$, at cessation $n = 5$), SMK+abx (at smoke exposure $n = 15$, at cessation $n = 5$), HFD-fed mice, three-way during smoke exposure and cessation, mean values. **(b)** Weight change during smoke exposure and cessation. HFD-fed mice, Non-SMK and Non-SMK+abx ($n = 10$), SMK, SMK+abx and SMK+abx at cessation ($n = 9$), mean ± s.e.m. For (**b**–**d**): last day: one-way ANOVA and Sidak correction. Inset: iAUC, one-way ANOVA and Sidak correction, mean ± s.e.m. **(c)** Weight change during smoke exposure and cessation in mice exposed to low-nicotine cigarette smoke and fed with HFD. Non-SMK, SMK and Non-SMK+abx ($n = 10$), SMK+abx ($n = 9$), mean ± s.e.m**. (d)** Weight change during smoke exposure and cessation. HFD-fed mice were implanted with osmotic pumps containing vehicle (PBS) or 0.5 mg/kg/day varenicline (var). Non-SMK and Non-SMK+var ($n = 5$), SMK and SMK+var ($n = 10$), mean ± s.e.m. Grey background in graphs refers to cessation period. *P<0.05; **P<0.01; ***P<0.001; ****P<0.0001, exact P values presented in Supplementary Table 1.

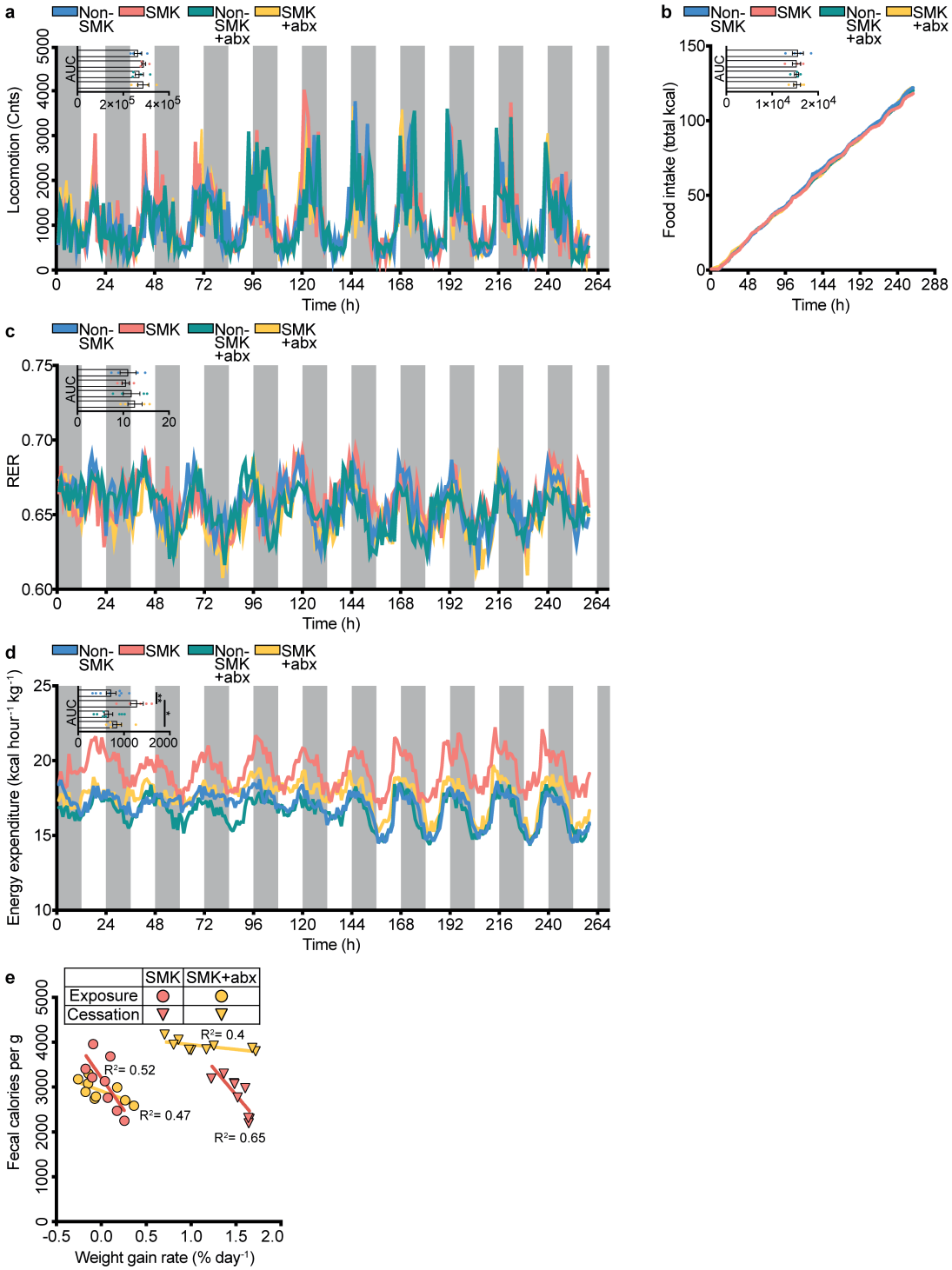

Extended Data Fig. 3 | Metabolic impacts of antibiotics treatment on SCWG. (a–c) Metabolic cage analysis during smoke exposure cessation over a period of 260h, $n = 4$ for all mice groups, HFD-fed mice. Locomotion **(a**, 'cnts' refers to light beam break count**)**, food intake **(b**, total kcal**)**, respiratory exchange ratio **(c**, RER**)**; inset: AUC (baseline = 0, baseline of RER = 0.7). One-way ANOVA and Sidak correction, mean ± s.e.m. **(d)** Energy expenditure analysis during cessation over a period of 260h. Non-SMK and Non-SMK+abx ($n = 8$), SMK ($n = 5$), SMK+abx ($n = 6$). Inset: AUC (baseline= minimum score, 14.1), One-way ANOVA and Sidak correction, mean ± s.e.m. **(e)** Pearson correlation between fecal calories and weight gain rate, smoke exposure (circles) and cessation (triangles). SMK (smoke exposure period $n = 8$, cessation period $n = 9$, red), SMK+abx (smoke exposure period $n = 9$, cessation period $n = 9$, yellow). Lines represent linear regression slopes and intercepts. Grey background in graphs refers to the dark cycle. *P<0.05; **P<0.01; exact P values presented in Supplementary Table 1.

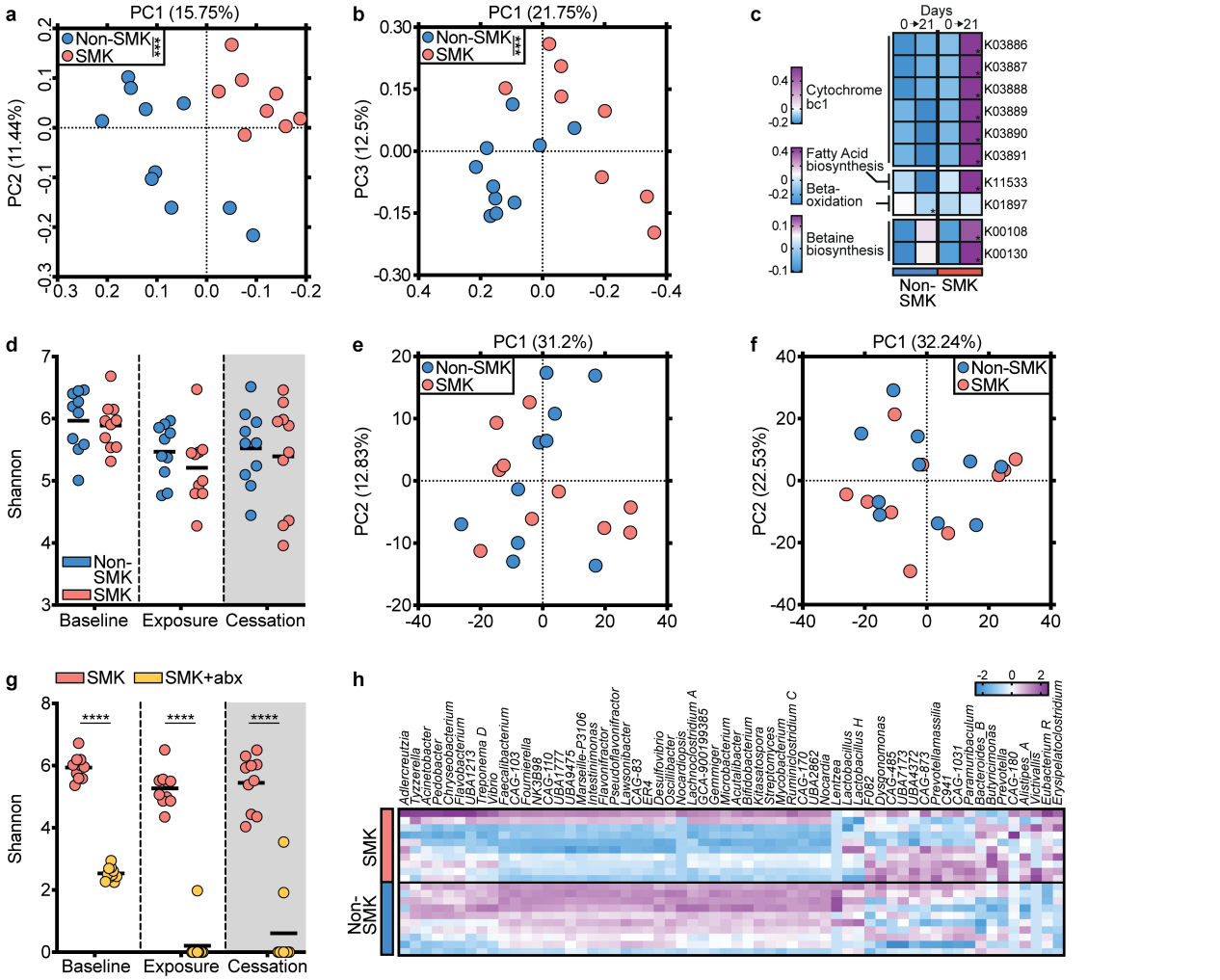

Extended Data Fig. 4 | Microbiome changes during smoke exposure and cessation. (**a**–**b**) 16S rDNA-based principal coordinate analysis (PCoA) for (**a**) Bray-Curtis dissimilarity or (**b**) Jaccard similarity for HFD-fed Non-SMK and SMK mice at day 21 (smoke exposure). Non-SMK ($n = 10$), SMK ($n = 8$) mice. Inset: PERMANOVA. **(c)** KEGG modules fully covered by KEGG orthologs that significantly differed upon comparisons between day 0 and day 21. HFD-fed mice, Non-SMK ($n = 10$ for all times), SMK ($n = 10$ for day 0, $n = 8$ for day 21); asterisks denote significant differences between day 21 versus day 0 for each group ($Q < 0.1$); two-sided Mann-Whitney *U*-test with BKY correction. **(d)** Alpha diversity quantified as Shannon index in fecal samples at day 0 (baseline), 21 (smoke exposure) and 35 (cessation). HFD-fed mice, Non-SMK and SMK $n = 10$ mice per group; PERMANOVA, mean values. **(e**–**f)** PCA of species-level relative abundance at day 0 **(e**, baseline**)** and day 35 **(f**, cessation**)**, HFD-fed mice $n = 10$ per group; inset: PERMANOVA. **(g)** Alpha diversity quantified as Shannon index in fecal samples at day 0 (baseline), 21 (smoke exposure) and 35 (cessation). HFD-fed mice, SMK ($n = 10$ for all times), SMK+abx ($n = 10$ at days 0 and 21, $n = 9$ at day 35); PERMANOVA, mean values. **(h)** Heatmap representing differentially abundant bacteria (genus level) in HFD-fed Non-SMK versus SMK mice at day 21 (smoke exposure). $n = 10$ mice per group; DESeq2; coloured bar represents *z* score. *$P<0.05$; ***$P<0.001$; ****$P<0.0001$, exact *P* values presented in Supplementary Table 1.

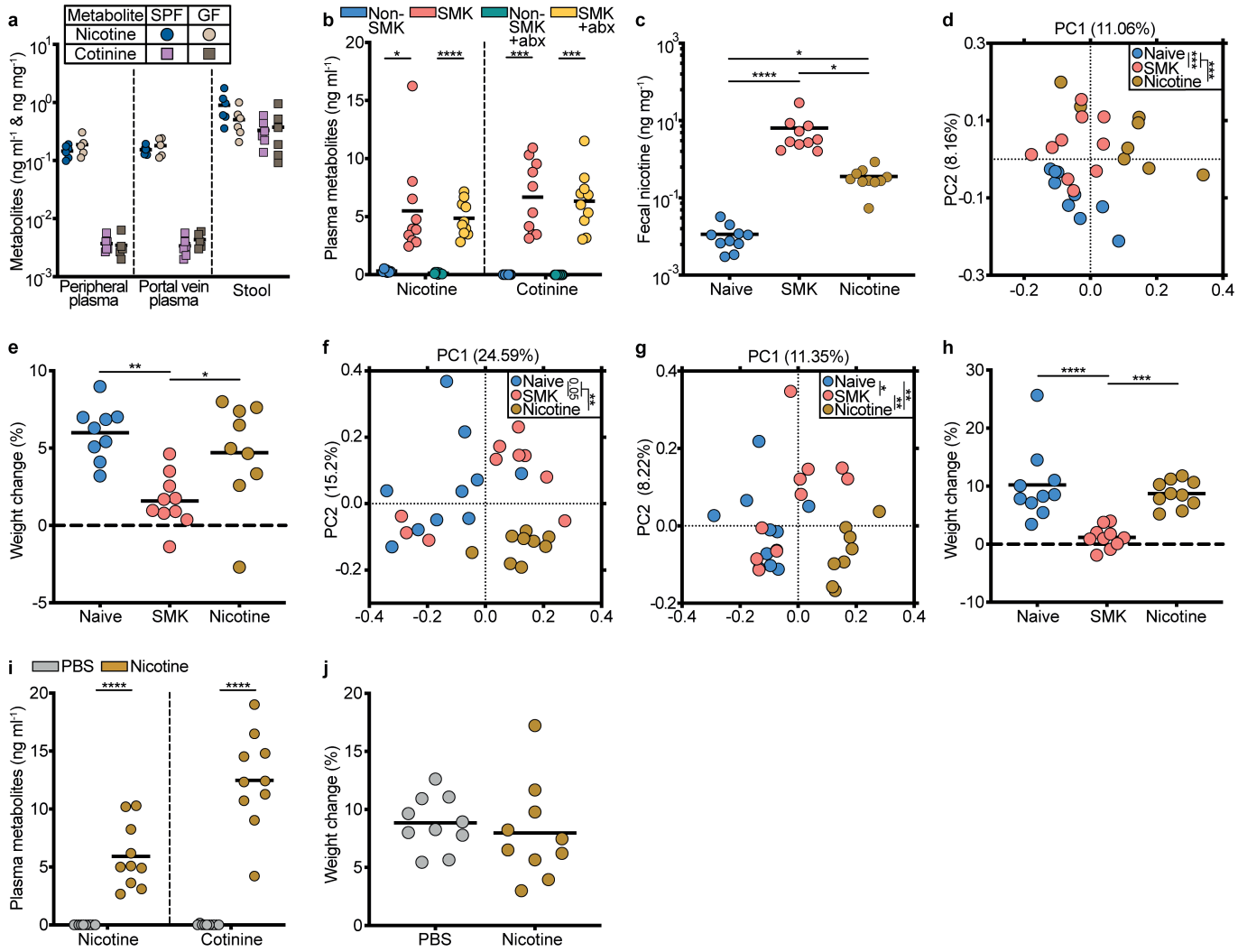

Extended Data Fig. 5 | Nicotine impacts on the microbiome and SCWG. **(a)** Nicotine and cotinine levels in peripheral plasma, portal vein plasma and stool in naive SPF and GF mice. SPF ($n = 6$), GF ($n = 5$ for plasma and portal vein, $n = 6$ for stool); two-sided Mann-Whitney *U* test, mean values. **(b)** Plasma nicotine and cotinine levels during smoke exposure. Non-SMK ($n = 8$), SMK and SMK+abx ($n = 10$), Non-SMK+abx ($n = 9$), HFD-fed mice, Kruskal-Wallis and Dunn's test, mean values. **(c)** Fecal nicotine levels in HFD-fed mice exposed for 3 weeks to cigarettes smoke or to nicotine by intra-peritoneal (i.p.) injections; $n = 10$ mice per group; Kruskal-Wallis and Dunn's test, mean values. **(d)** PCoA depicting Jaccard similarity in mice exposed to cigarette smoke or to i.p. nicotine; Naive ($n = 9$), SMK ($n = 10$), nicotine-administered (i.p., $n = 8$) mice; pairwise PERMANOVA. **(e)** Weight change in mice exposed to cigarette smoke or to i.p. nicotine; Naïve and nicotine ($n = 9$), SMK ($n = 10$); day 21: one-way ANOVA and Tukey correction, mean values. **(f–g)** 16S rDNA-based PCoA depicting (**f**) Bray-Curtis dissimilarity and (**g**) Jaccard distance; Naive and SMK ($n = 10$), nicotine-administered *via* drinking water ($n = 9$), pairwise PERMANOVA. **(h)** Weight change in mice exposed for 3 weeks to cigarette smoke or to nicotine *via* drinking water. Naive and SMK ($n = 10$) nicotine ($n = 9$); day 21: one-way ANOVA and Tukey correction, mean values. **(i)** Plasma levels of nicotine and cotinine in HFD-fed mice administered with PBS or nicotine by osmotic pumps for 3 weeks, $n = 10$ mice per group; two-sided Mann-Whitney *U*-test, mean values. **(j)** Weight change in HFD-fed mice administered with PBS or nicotine by osmotic pumps for 4 weeks. $n = 10$ mice per group; day 28: unpaired two-sided *t*-test, mean values. *$P<0.05$; **$P<0.01$; ***$P<0.001$; ****$P<0.0001$, *P* values presented in Supplementary Table 1.

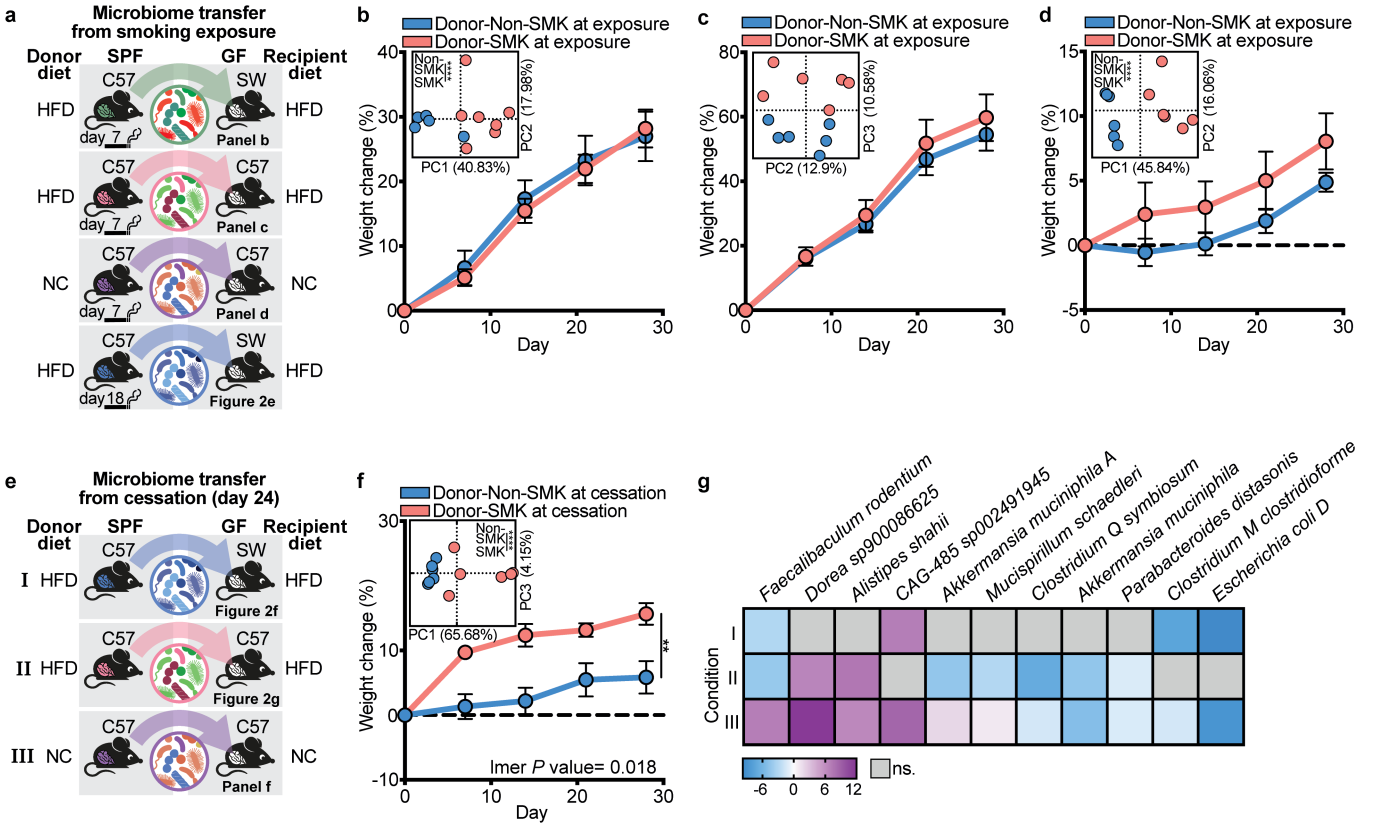

Extended Data Fig. 6 | Fecal microbiome transplantation (FMT) from mice exposed to smoke. (a) Experimental scheme of FMT experiments performed using fecal donations from mice exposed to smoke. Fecal samples from Non-SMK and SMK mice at day 7 (early smoke exposure) or day 18 (during smoke exposure) were transferred into GF mice of the designated strains, fed with the designated diets. **(b–d)** Weight change of GF mice following FMT. Fecal donations were collected at day 7 from HFD-fed C57BL/6 mice. For **b**, **c**, **d**, **f**: day 28, unpaired two-sided *t*-test, mean ± s.e.m.; upper inset: shotgun metagenomic sequencing showing PCA of species composition (for b Non-SMK $n = 5$, SMK $n = 7$ mice, for c, d, f $n = 6$ mice per group), PERMANOVA. **(b)** Recipients: HFD-fed SW mice. Non-SMK ($n = 11$), and SMK ($n = 13$) mice; day 28: unpaired two-sided *t*-test, mean ± s.e.m. **(c)** Recipients: HFD-fed C57BL/6 mice. Non-SMK ($n = 7$) and SMK ($n = 6$) mice, mean ± s.e.m. **(d)** Recipients: NC-fed C57BL/6 mice, $n = 6$ mice per group, mean ± s.e.m. **(e)** Experimental scheme of FMT experiments performed during cessation. Fecal samples from Non-SMK and SMK mice at day 24 (cessation) were transferred into GF mice of the designated strains, fed the designated diets. **(f)** Weight change of GF mice receiving FMT from C57BL/6 NC-fed mice at day 4 of cessation (total day 24). Recipients: NC-fed C57BL/6 mice, $n = 6$ mice per group, mean ± s.e.m. **(g)** Heatmap presenting log2 fold change of bacteria that were significantly changed ($Q < 0.05$) at least in two conditions (presented in Extended Data Fig. 6e); DESeq2; ns.: non-significant; coloured bar represents log fold change. $^{*}P<0.05$; $^{**}P<0.01$, $^{****}P<0.0001$, exact *P* values presented in Supplementary Table 1.

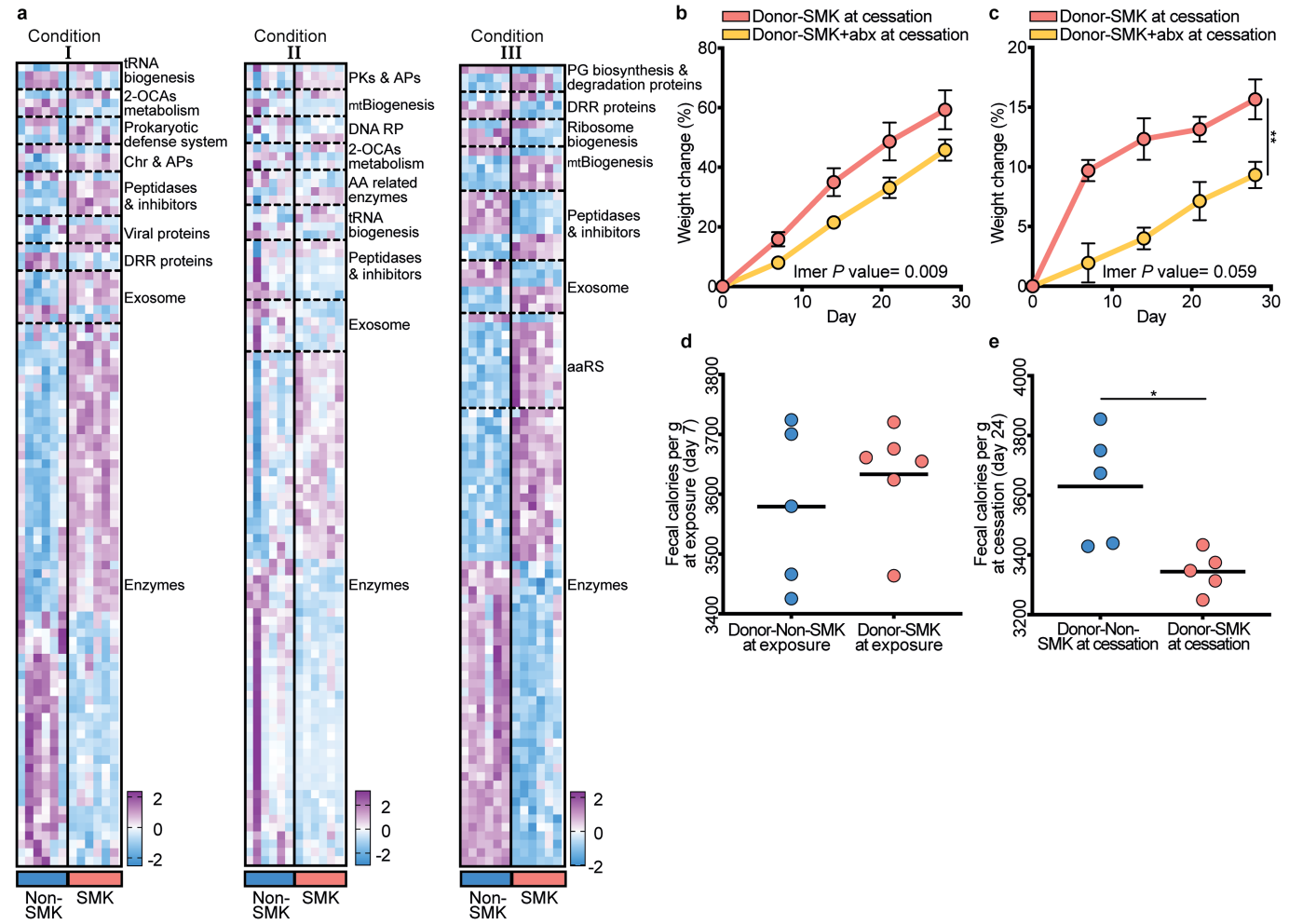

Extended Data Fig. 7 | Functional features of transplanted microbiomes from mice exposed to smoke and at cessation. (a) Heatmaps describing the functional potential of metagenomic features (EC annotated) in shotgun metagenomics, corresponding to the conditions of Extended Data Fig. 6e. Features were grouped according to BRITE hierarchy; colored bar represents *z* score. **(b–c)** Weight change of GF C57BL/6 mice following FMT. Fecal donations were collected at day 24 of smoke exposure and cessation from abx-treated or untreated HFD-fed C57BL/6 mice (**b**) or NC (**c**); Day 28, unpaired two-sided *t*-test, mean ± s.e.m. **(b)** Recipients: HFD-fed C57BL/6 mice, SMK ($n = 7$) and SMK+abx ($n = 6$), mean ± s.e.m. **(c)** Recipients: NC-fed C57BL/6 mice, $n = 6$ per group, mean ± s.e.m. **(d–e)** Fecal calories of GF recipients after FMT from early smoke exposure (**d**, Non-SMK $n = 5$, SMK $n = 6$) or cessation (**e**, $n = 5$ mice per group); unpaired two-sided *t*-test, mean values. $^*P<0.05$, $^{**}P<0.01$, *P* values presented in Supplementary Table 1.

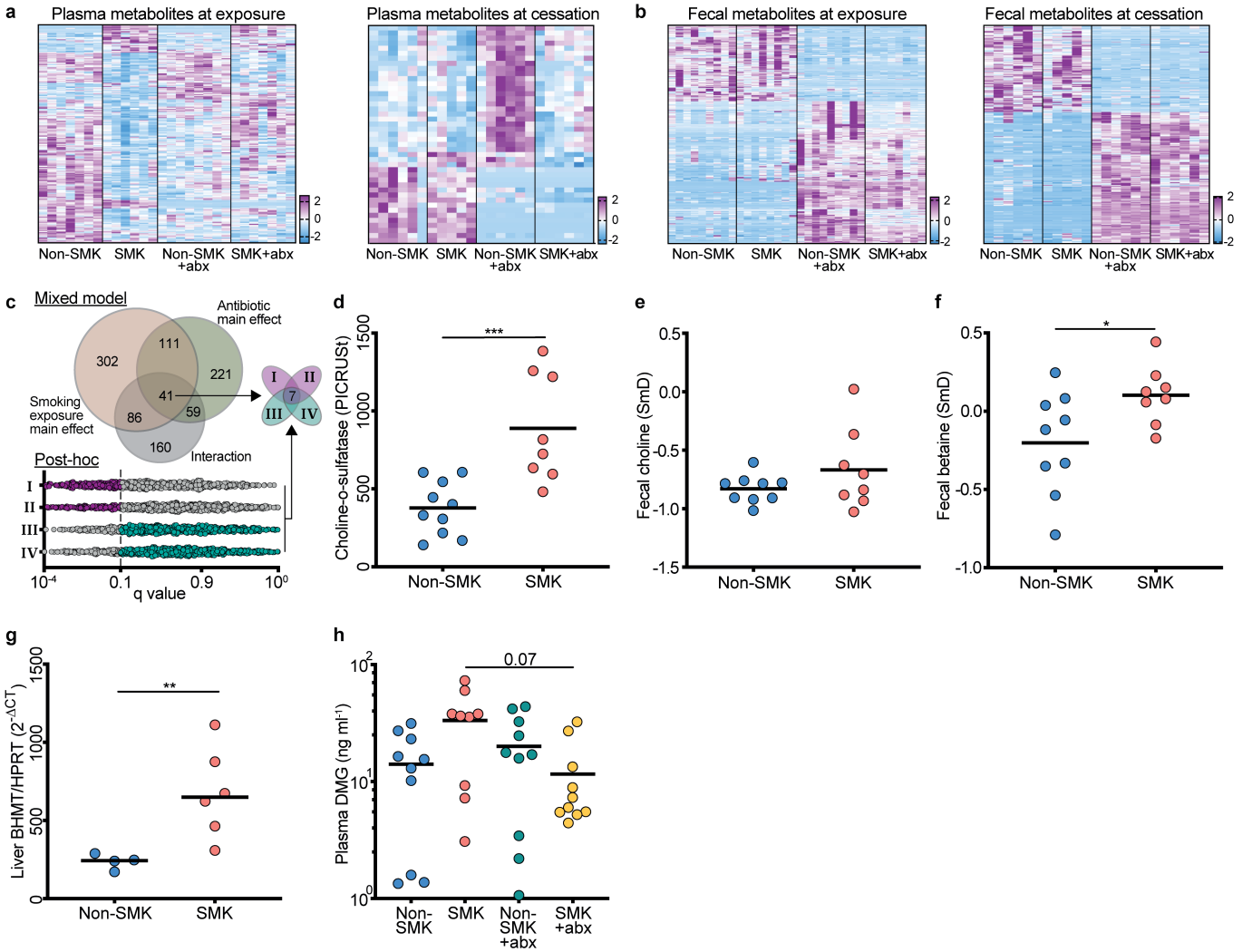

Extended Data Fig. 8 | Candidate metabolites associated with SCWG. **(a)** Heatmaps depicting plasma metabolites of HFD-fed mice during smoke exposure (day 15) and cessation (day 30). Non-SMK, SMK+abx ($n = 7$ smoke exposure, $n = 6$ cessation), SMK ($n = 6$ smoke exposure, $n = 5$ cessation), Non-SMK+abx ($n = 8$ smoke exposure, $n = 6$ cessation); heatmap intensities represent normalized metabolite levels (z-score). **(b)** Heatmaps depicting fecal metabolites during smoke exposure (day 21) and cessation (day 35). Non-SMK and Non-SMK+abx ($n = 9$ for smoke exposure and $n = 6$ for cessation), SMK ($n = 8$ for smoke exposure and $n = 5$ for cessation) and SMK+abx ($n = 8$ for smoke exposure and $n = 6$ for cessation) HFD-fed mice; heatmap intensities represent normalized metabolite levels (z-score). **(c)** LMM, utilizing both smoke and antibiotics alterations throughout time and quantifying their interactive impacts on plasma metabolite levels at smoke exposure. Venn diagram (left) represents significant ($p<0.05$) metabolites impacted by smoke exposure, antibiotics and their interactions. Post-hoc: Tukey correction for multiple comparisons. Venn diagram (right): metabolites fulfilling both mixed linear model and statistical hypothesis testing criteria. **(d)** Predicted gene copy numbers (PICRUSt2) of fecal choline sulfatase: Non-SMK ($n = 10$), SMK ($n = 8$) HFD-fed mice; unpaired two-sided t-test; mean values. **(e-f)** Fecal metabolites, untargeted mass spectrometry, HFD-fed mice, Non-SMK ($n = 9$), SMK ($n = 8$ at smoke exposure), unpaired two-sided t-test, mean ± s.e.m. values of (**e**) choline and (**f**) betaine; SmD- scaled imputed data, log scale values (methods). **(g)** qPCR quantification of liver betaine-homocysteine S-methyltransferase (BHMT) transcripts during smoke exposure. HFD-fed mice, Non-SMK ($n = 4$), SMK ($n = 6$); two-sided Mann-Whitney U-test, mean ±s.e.m. **(h)** Plasma DMG levels, assessed by targeted mass spectrometry. Non-SMK, Non-SMK+abx and SMK+abx ($n = 10$), SMK ($n = 9$), mice fed with HFD; Kruskal-Wallis and Dunn's test, mean values. *$P<0.05$, **$P<0.01$, exact P values presented in Supplementary Table1.

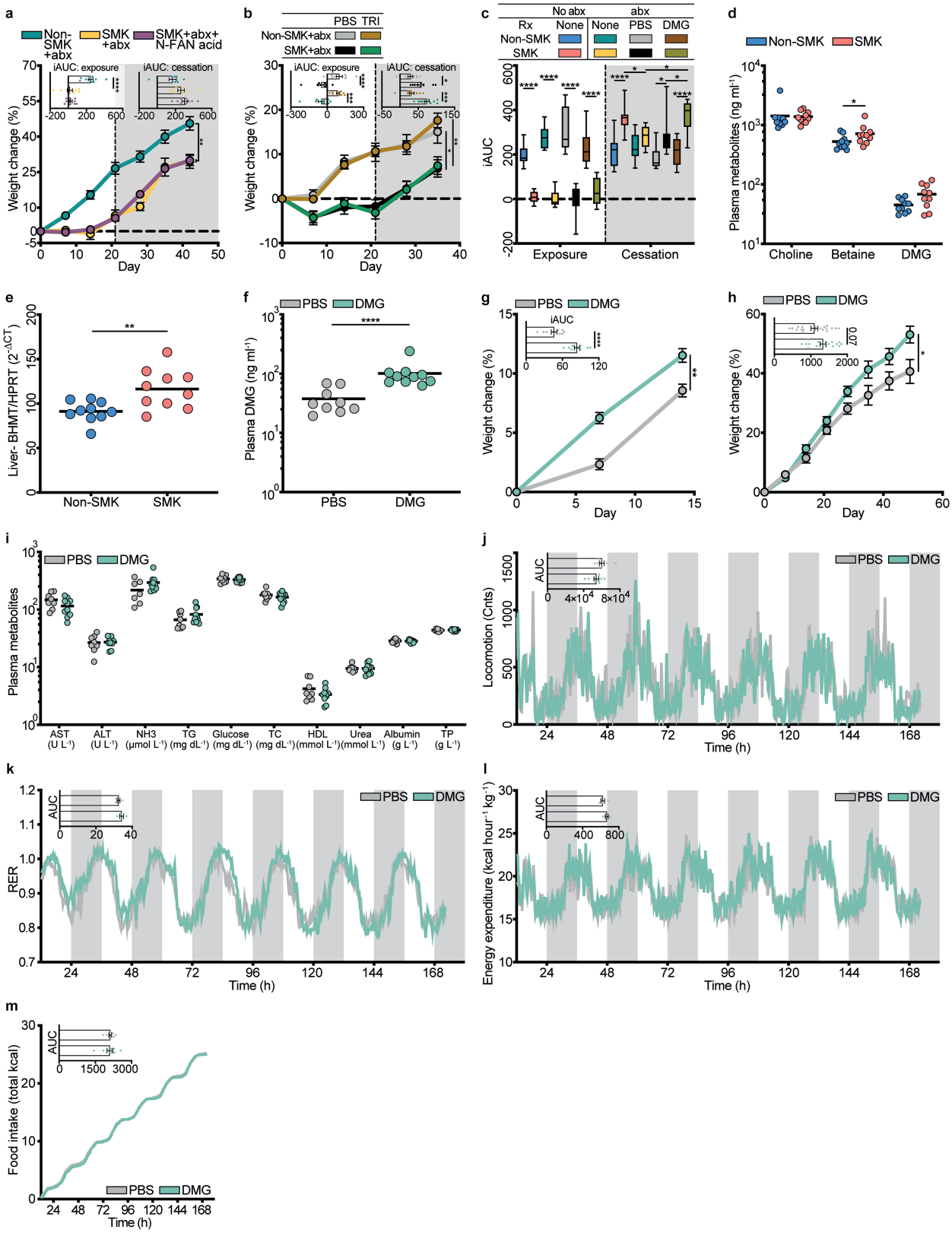

Extended Data Fig. 9 | See next page for caption.

Extended Data Fig. 9 | Metabolite impacts on SCWG. (a–b) Weight change during smoke exposure and cessation upon addition of N-formylanthranilic acid **(a**, N-FAN acid**)** or trigonelline **(b**, TRI**). a**: $n = 10$ HFD-fed mice per group, mean ± s.e.m; day 42: unpaired 2-sided *t* test; iAUC: unpaired 2-sided *t* test, mean ± s.e.m. **b**: Non-SMK+abx+PBS, Non-SMK+abx+TRI and SMK+abx+TRI ($n = 10$), SMK+abx+PBS ($n = 9$), HFD-fed mice, mean ± s.e.m; day 35: one-way ANOVA Sidak correction; inset: iAUC; one-way ANOVA Sidak correction, mean ± s.e.m. **(c)** iAUC of weight change at smoke exposure or cessation of Fig 4a. NS+abx ($n = 9$), SMK+abx+PBS ($n = 10$ smoke exposure, $n = 9$ cessation), all other groups $n = 10$; one-way ANOVA Sidak correction; box plots represent max-min values. Rx- treatment. **(d)** Plasma levels of metabolites of the DMG biosynthesis pathway assessed by targeted mass spectrometry in mice consuming choline-deficient diet (CDD), $n = 10$; two-sided Mann-Whitney *U*-test, mean values. **(e)** Hepatic BHMT qPCR during smoke exposure in mice consuming CDD, $n = 10$; unpaired two-sided t-test, mean values. **(f)** Targeted mass spectrometry of plasma DMG. PBS ($n = 9$), DMG ($n = 10$) HFD-fed mice; two-sided Mann-Whitney *U*-test, mean values. **(g–h)** Weight change during DMG supplementation on day 14 **(g**, $n = 10$**)** or day 49 **(h**, PBS: $n = 19$, DMG: $n = 18$, pool of 2 independent repeats**)**, mean ± s.e.m., HFD-fed mice; last time point: unpaired two-sided *t*-test. Inset: iAUC, unpaired two-sided *t*-test, mean ± s.e.m. **(i)** Plasma levels of HFD-fed mice treated with PBS ($n = 8$ for all paraments except $n = 7$ for NH_3) or DMG ($n = 10$ for all parameters except $n = 9$ for ALT); unpaired two-sided *t*-test, except two-sided Mann Whitney *U* test for NH_3 and HDL; mean values. **(j–m)** Metabolic cage analysis for 172h in DMG versus PBS supplemented mice. Locomotion **(j**, $n = 8$**)**, respiratory exchange ratio **(k**, RER, $n = 4$**)**, energy expenditure **(l**, $n = 4$**)** and food intake (Total kcal, **m**, $n = 8$**)**. Inset: AUC; unpaired two-sided *t*-test, mean ± s.e.m. Grey background depicts the cessation period (a–c) or the dark cycle (j–i). $^{*}P<0.05$; $^{**}P<0.01$; $^{***}P<0.001$; $^{****}P<0.0001$, *P* values presented in Supplementary Table 1.

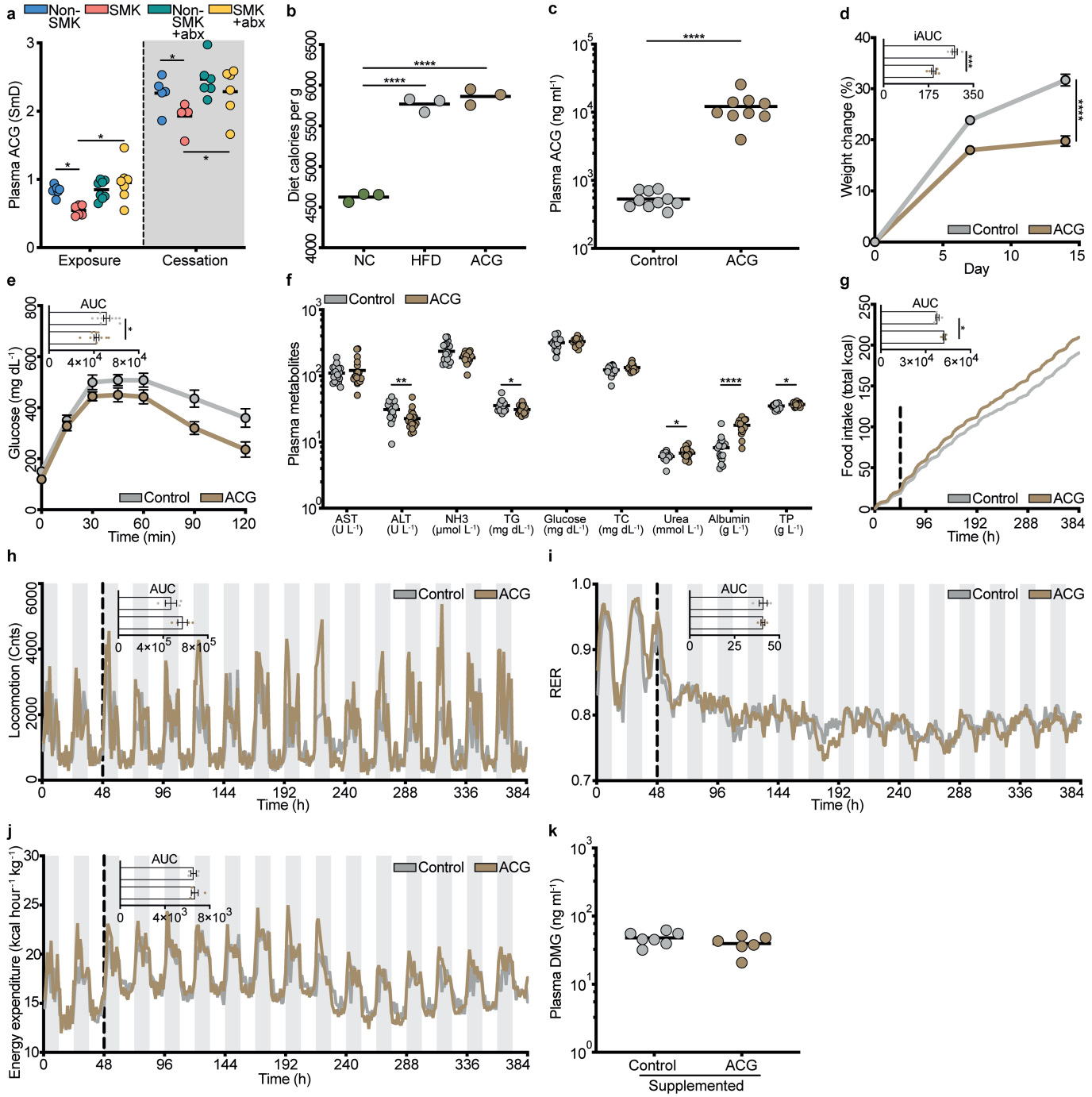

Extended Data Fig. 10 | ACG supplementation ameliorates weight gain. **(a)** Plasma levels of ACG during smoke exposure (day 15) and cessation (day 30). Non-SMK ($n = 7$ for smoke exposure, $n = 5$ for cessation), SMK ($n = 6$ for smoke exposure, $n = 5$ for cessation), Non-SMK+abx ($n = 8$ for smoke exposure, $n = 6$ for cessation), SMK+abx ($n = 7$ for smoke exposure, $n = 6$ for cessation), HFD-fed mice; two-way ANOVA and BH correction ($Q < 0.1$), mean values. **(b)** Calories measured in rodent diet. $n = 3$ mice per group; one-way ANOVA and Tukey correction, mean values. **(c)** Plasma levels of ACG in HFD (Control, $n = 10$) or HFD+ACG (ACG, $n = 9$) mice, assessed by targeted mass spectrometry. Unpaired two-sided *t*-test, mean values. **(d)** Weight change during ACG supplementation. $n = 5$ HFD-fed mice per group, mean ± s.e.m.; day 14: unpaired two-sided *t*-test. Inset: iAUC, unpaired two-sided *t*-test, mean ± s.e.m. **(e)** GTT during ACG administration (day 49) $n = 10$ HFD-fed mice per group. Inset: AUC, Unpaired two-sided *t*-test, mean ± s.e.m. **(f)** Plasma biochemical levels Control ($n = 19$ except $n = 17$ for TG & urea, $n = 18$ for albumin). ACG ($n = 19$ except for $n = 18$ for NH3) HFD-fed mice. Two-sided Mann-Whitney *U*-test, except for unpaired two-sided *t*-test for glucose, total cholesterol, urea and total protein, mean values. **(g–j)** Metabolic cage analysis for 384h, $n = 4$ HFD-fed mice per group, dashed line indicates the starting day of the diet. **(g)** Food intake (total kcal); **(h)** locomotion ('cnts' refers to light beam break count); **(i)** respiratory exchange ratio (RER); and **(j)** energy expenditure; inset: AUC, unpaired two-sided *t*-test except two-sided Mann-Whitney *U*-test for energy expenditure, mean ± s.e.m. Grey background depicts the dark cycle. **(k)** Plasma DMG levels in Control ($n = 7$) or ACG ($n = 6$) mice, unpaired two-sided *t*-test, mean values. *$P<0.05$; **$P<0.01$; ***$P<0.001$; ****$P<0.0001$, exact *P* values presented in Supplementary Table 1.

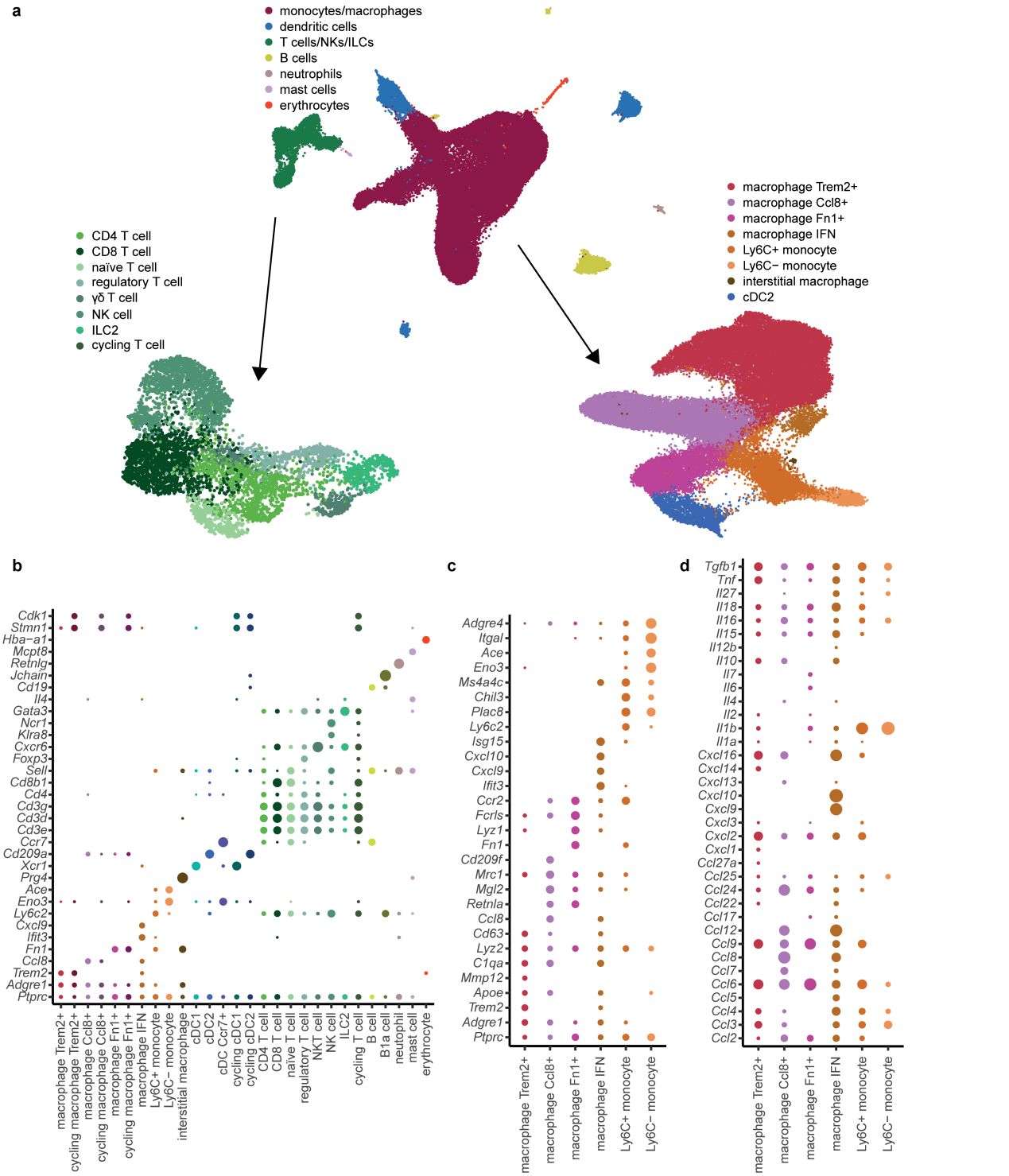

Extended Data Fig. 11 | Single cell transcriptomic analysis of adipose tissue immune cells of HFD-fed, DMG- and ACG-supplemented mice not exposed to smoke. **(a)** UMAP representation of single cell data showing stepwise clustering of adipose immune cell populations. **(b)** Balloonplot showing the mean of normalized and scaled gene expression of key markers used to annotate clusters to cell types. **(c)** Balloonplot showing the mean of normalized and scaled gene expression of key markers of macrophage and monocyte populations. **(d)** Balloonplot showing the mean of normalized and scaled gene expression of key markers of chemokines and cytokines in macrophage and monocyte populations. A larger size of the dot in the balloonplot represent increased expression. See Supplementary Table 6 for single cell transcriptomic data.

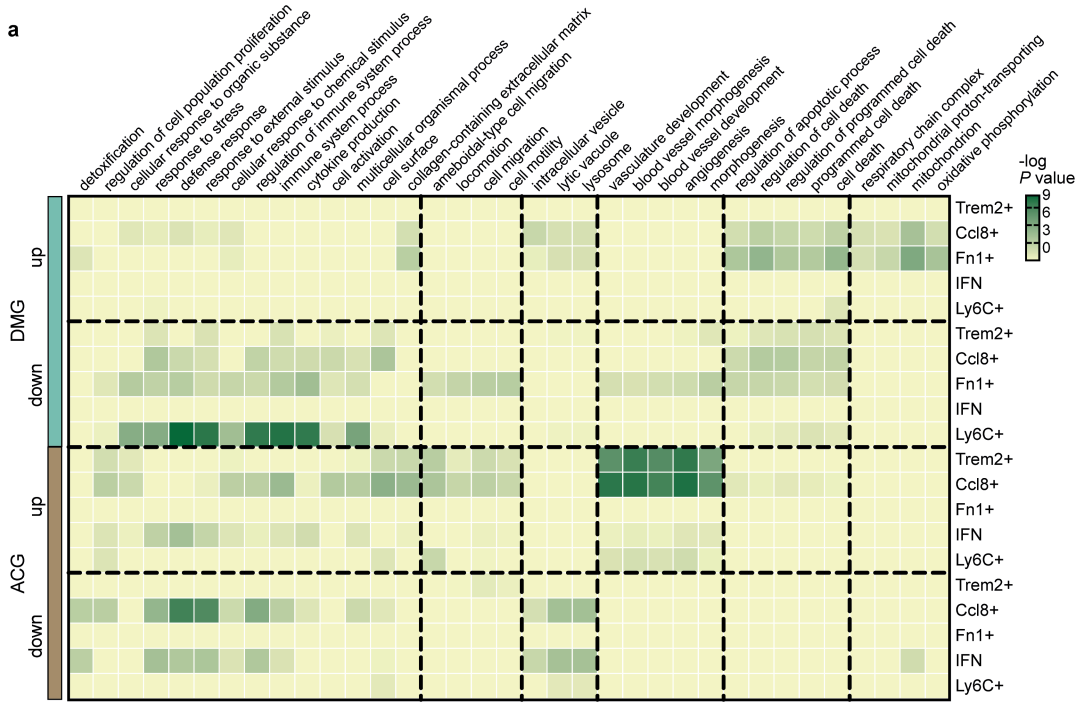

Extended Data Fig. 12 | Adipose tissue immune cell features of HFD-fed, DMG- and ACG-supplemented mice not exposed to smoke. (a) Heatmap showing -log10 of BH adjusted p-value GO functional enrichment analysis of genes differentially expressed in macrophage subpopulations upon treatment with ACG and DMG. See Supplementary Table 6 for single cell transcriptomic data.

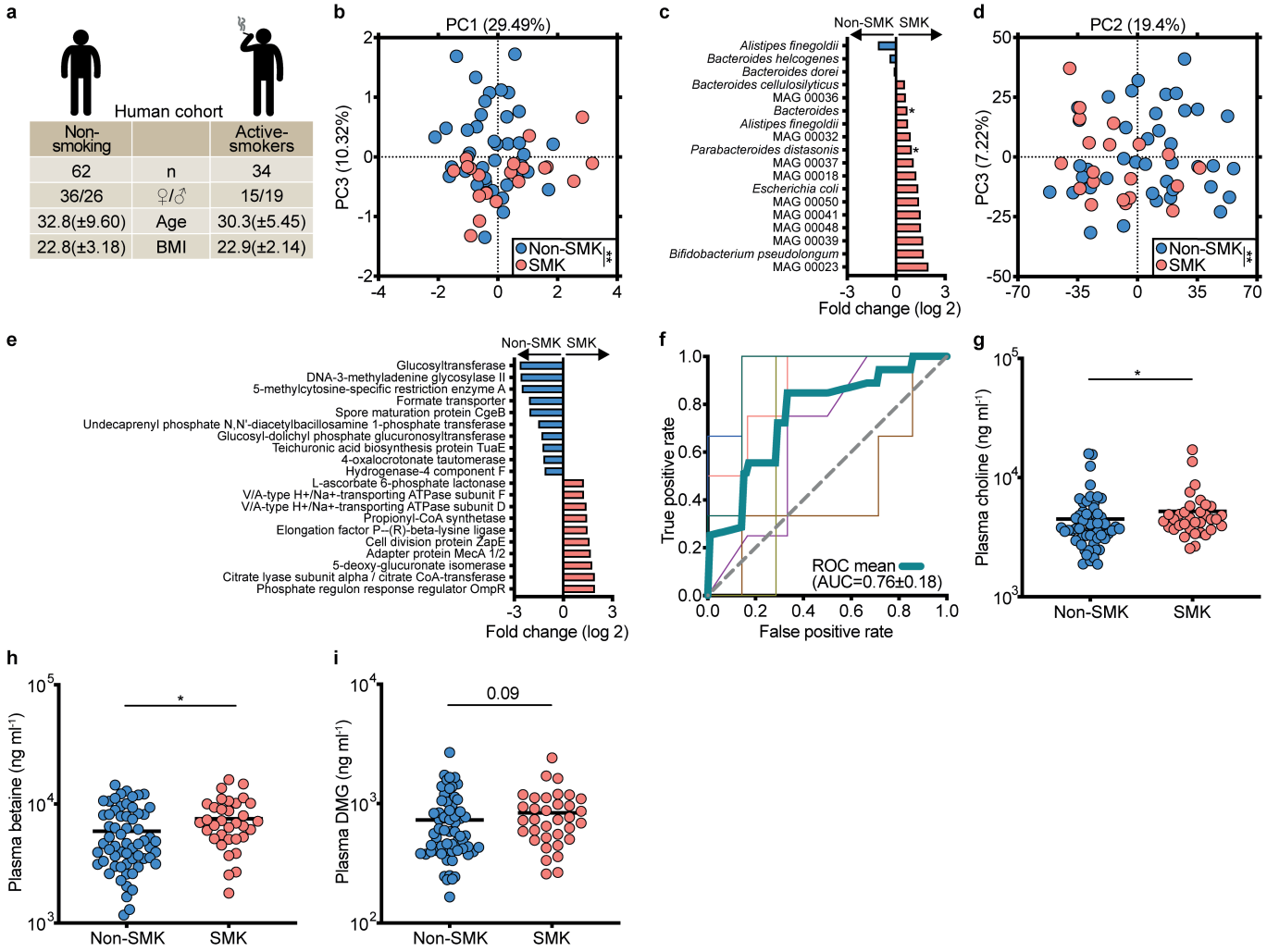

Extended Data Fig. 13 | Potential microbiome and metabolite associations with human who smoke. (a) Experimental outline of the human cohort. **(b–f)** human fecal microbiome analysis (Non-SMK $n = 40$, SMK $n = 20$). **(b)** PCA of metagenomically-assembled genomes (MAGs) relative abundances in human stool; inset: PERMANOVA. **(c)** Differentially abundant MAGs; asterisks denote significant differences ($p<0.05$); two-sided Mann-Whitney *U*-test. **(d)** PCA of KO annotated reads; inset: PERMANOVA. **(e)** KEGG orthologs of highest effect (feature with negative values enriched in SMK), two-sided Mann-Whitney *U*-test, highest (and lowest), 2-fold log change. **(f)** ROC curves for binary classifier (methods). **(g–i)** Targeted mass spectrometry of metabolites from the DMG biosynthesis pathway: choline (**g**), betaine (**h**) and DMG (**i**); Non-SMK ($n = 62$), SMK ($n = 34$); two-sided Mann-Whitney *U*-test, mean values. *$P<0.05$; **$P<0.01$, exact *P* values presented in Supplementary Table 1, raw data presented in Supplementary Table 7.

nature research

Corresponding author(s): Eran Elinav

Last updated by author(s): Nov, 25, 2021

Reporting Summary

Nature Research wishes to improve the reproducibility of the work that we publish. This form provides structure for consistency and transparency in reporting. For further information on Nature Research policies, see our Editorial Policies and the Editorial Policy Checklist.

Statistics

For all statistical analyses, confirm that the following items are present in the figure legend, table legend, main text, or Methods section.

n/a	Confirmed
☐	☒ The exact sample size (*n*) for each experimental group/condition, given as a discrete number and unit of measurement
☐	☒ A statement on whether measurements were taken from distinct samples or whether the same sample was measured repeatedly
☐	☒ The statistical test(s) used AND whether they are one- or two-sided *Only common tests should be described solely by name; describe more complex techniques in the Methods section.*
☐	☒ A description of all covariates tested
☐	☒ A description of any assumptions or corrections, such as tests of normality and adjustment for multiple comparisons
☐	☒ A full description of the statistical parameters including central tendency (e.g. means) or other basic estimates (e.g. regression coefficient) AND variation (e.g. standard deviation) or associated estimates of uncertainty (e.g. confidence intervals)
☐	☒ For null hypothesis testing, the test statistic (e.g. *F*, *t*, *r*) with confidence intervals, effect sizes, degrees of freedom and *P* value noted *Give P values as exact values whenever suitable.*
☒	☐ For Bayesian analysis, information on the choice of priors and Markov chain Monte Carlo settings
☒	☐ For hierarchical and complex designs, identification of the appropriate level for tests and full reporting of outcomes
☒	☐ Estimates of effect sizes (e.g. Cohen's *d*, Pearson's *r*), indicating how they were calculated

Our web collection on statistics for biologists contains articles on many of the points above.

Software and code

Policy information about availability of computer code

Data collection	No software was used
Data analysis	bcl2fastq 2.17.1.14, Qiime2 2019.07.0, Anvio's (master branch, commit no. 17ff1a437118a402c2934ed68e111bc8d1f1e0d9), MEGAHIT 1.2.9, scipy 0.19.1, matplotlib 2.0.2, seaborn 0.9.0, scikit-learn 0.20.0, pandas 0.20.3, numpy 1.15.1., DESeq2 1.24.0 Seurat v.3.2.3, Cell Ranger v.6.0.0, gprofiler2 v.0.2.0

For manuscripts utilizing custom algorithms or software that are central to the research but not yet described in published literature, software must be made available to editors and reviewers. We strongly encourage code deposition in a community repository (e.g. GitHub). See the Nature Research guidelines for submitting code & software for further information.

Data

Policy information about availability of data

All manuscripts must include a data availability statement. This statement should provide the following information, where applicable:

- Accession codes, unique identifiers, or web links for publicly available datasets
- A list of figures that have associated raw data
- A description of any restrictions on data availability

Metagenomic sequences and resolved MAGs are available at the European Nucleotide Archive under project accession number PRJEB40095 at https://www.ebi.ac.uk/ena/browser/view/PRJEB40095. Single-cell RNA raw sequences are deposited in ArrayExpress with accession E-MTAB-10869 at https://www.ebi.ac.uk/arrayexpress/experiments/E-MTAB-10869. Metabolomic data are provided in Supplementary Table 4 and in the publicly accessible platform of Mendeley at https://doi.org/10.17632/539zh45tw2.1.

Field-specific reporting

Please select the one below that is the best fit for your research. If you are not sure, read the appropriate sections before making your selection.

☒ Life sciences ☐ Behavioural & social sciences ☐ Ecological, evolutionary & environmental sciences

For a reference copy of the document with all sections, see nature.com/documents/nr-reporting-summary-flat.pdf

Life sciences study design

All studies must disclose on these points even when the disclosure is negative.

Sample size	The minimal sample size for each experiment was set by the minimal number of mice allowed in a cage, taking into account that each group must includ at least 2 cages in order to control for cage effect. For example, an experiment with two groups at least 16 mice were included (4 mice per cage, 2 cages per group). Considering the low variability within a cage and group, taking into account the uniform genetic background of the mice in each experimental setting, combined with the fact that independent repetitions of the different experiments resulted in highly consistent results - we used the specified size number for each experiment.
Data exclusions	For the human cohort, subjects with no metagenomic samples with depth > 8M reads were omitted from the analysis. For mice 16S rDNA data, samples that did not reach the established sequencing depths (44,946, 50,173 and 30,014 reads for the smoke exposure, intra-peritoneal nicotine and oral nicotine experiments, respectively) were excluded from further analysis.
Replication	The results of all repetitions are reported in source data tables and the repetitions are indicated along the text and in the legends of each figure. Metabolomics profiling, shotgun and 16S sequencing, and single cell RNA-seq were done for a single independent experimental repetition.
Randomization	For all experiments, mice were randomly assigned to each group based on their weight in order to eliminate weight differences at baseline. For the human experiments, data was obtained from an on-going clinical trial in our lab, and subjects were allocated to groups according to their active smoking status, without any intervention from our side. Confounding factors - age, sex, BMI - were tested in order to make sure the groups don't differ significantly with respect to these factors.
Blinding	Key experiments were repeated at least twice by different unbiased (blinded) investigators

Reporting for specific materials, systems and methods

We require information from authors about some types of materials, experimental systems and methods used in many studies. Here, indicate whether each material, system or method listed is relevant to your study. If you are not sure if a list item applies to your research, read the appropriate section before selecting a response.

Materials & experimental systems

n/a	Involved in the study
☒	☐ Antibodies
☒	☐ Eukaryotic cell lines
☒	☐ Palaeontology and archaeology
☐	☒ Animals and other organisms
☐	☒ Human research participants
☐	☒ Clinical data
☒	☐ Dual use research of concern

Methods

n/a	Involved in the study
☒	☐ ChIP-seq
☒	☐ Flow cytometry
☒	☐ MRI-based neuroimaging

Animals and other organisms

Policy information about studies involving animals; ARRIVE guidelines recommended for reporting animal research

Laboratory animals	8-weeks old C57BL/6J male mice purchased from Envigo (or Jackson laboratory, specifically for one experiment) and allow to be adjusted for 2 weeks before experimentation. Mice were housed at the animal facility, Weizmann Institute of Science, in a specific pathogen-free animal facility at an ambient temperature of 22°C and 50% humidity, 12 light/12 dark cycle. Germ free mice were obtained from the germ-free facility, Weizmann Institute of Science.
Wild animals	Study did not involve wild animals
Field-collected samples	Study did not involve sample collection from the field
Ethics oversight	All experimental procedures involving mice were approved by the local IACUC no. 09890119-3.

Note that full information on the approval of the study protocol must also be provided in the manuscript.

Human research participants

Policy information about studies involving human research participants

Population characteristics	Ninety-six healthy volunteers were recruited for this study between the years 2018-2020. Age- and BMI-matched a non-smoking cohort (n= 62) and an actively smoking cohort (n= 34) were utilized. Blood and stool samples were collected from the participants followed targeted mass spectrometry and metagenomic sequencing respectively. For the metabolomics analysis, the non-smoking group contained 62 participants, 36 females and 26 males, with mean BMI 22.85 ± 3.18 (SD) and mean age of 32.8 ± 9.6, while the smoking participants group included 34 subjects, 15 females and 19 males, mean BMI of 22.98 ±2.14 and mean age of 30.3 ± 5.5 . The metagenomics analysis included only subjects with samples deeper than 8M reads, resulting in 60 subjects. The non-smoking group contained 40 participants, 21 females and 19 males, with mean BMI 22.3 ± 2.93 (SD) and mean age of 33.1 ±10.3, while the smoking participants group included 20 subjects, 7 females and 13 males, mean BMI of 23.45 ±2.29 and mean age of 29.71 ± 5.77 .
Recruitment	All subjects fulfilled the following inclusion criteria: males and females, aged 18-70, body mass index<28, who able to provide informed consent. Exclusion criteria included: (i) pregnancy or fertility treatments; (ii) usage of antibiotics or antifungals within 3 months prior to participation; (iii) consumption of probiotics or non-nutritive sweeteners within 1 month prior to participation, (iv) chronically active inflammatory, cardiovascular, infectious, endocrine or neoplastic disease within the three years prior to enrollment; (v) chronic gastrointestinal disorder, including inflammatory bowel disease and celiac disease and celiac disease, or gastrointestinal surgery such as bariatric surgery; (vi) neuropsychiatric disorder; (vii) coagulation disorders; (viii) pre-diagnosed type I or type II diabetes mellitus or treatment with anti-diabetic medications. (ix) Alcohol or substance abuse. Adherence to inclusion and exclusion criteria was validated by medical doctors. These data was obtained from an on-going unrelated clinical trial in our lab. Considering all available data were used - selection bias is not possible.
Ethics oversight	The observational human experiment was approved by the Weizmann Institute of Science Bioethics and Embryonic Stem Cell Research oversight committee (IRB approval number 170-2).

Note that full information on the approval of the study protocol must also be provided in the manuscript.

Clinical data

Policy information about clinical studies

All manuscripts should comply with the ICMJE guidelines for publication of clinical research and a completed CONSORT checklist must be included with all submissions.

Clinical trial registration	The observational human experiment was approved by the Weizmann Institute of Science Bioethics and Embryonic Stem Cell Research oversight committee (IRB approval number 170-2). https://clinicaltrials.gov/ct2/show/NCT03708939
Study protocol	https://clinicaltrials.gov/ct2/show/NCT03708939
Data collection	Participants were recruited for this study between the years 2018-2020
Outcomes	Blood and stool samples were collected from the participants followed targeted mass spectrometry and metagenomic sequencing respectively